FtsW activity and lipid II synthesis are required for recruitment of MurJ to midcell during cell division in *Escherichia coli*

Xiaolong Liu[1], Nils Y. Meiresonne[1], Ahmed Bouhss[2,3] and Tanneke den Blaauwen[1*]

[1]*Bacterial Cell Biology, Swammerdam Institute for Life Sciences, Faculty of Science, University of Amsterdam, Amsterdam, The Netherlands.*

[2]*Institute for Integrative Biology of the Cell (I2BC), CEA, CNRS, Univ Paris-Sud, Université Paris-Saclay, 91198, Gif-sur-Yvette, France.*

[3]*Laboratoire Structure-Activité des Biomolécules Normales et Pathologiques (SABNP), Univ Evry, INSERM U1204, Université Paris-Saclay, 91025 Evry, France*

*Corresponding author

Abstract

Peptidoglycan (PG) is the unique cell shape-determining component of the bacterial envelope, and is a key target for antibiotics. PG synthesis requires the transmembrane movement of the precursor lipid II, and MurJ has been shown to provide this activity in *E. coli*. However, how MurJ functions *in vivo* has not been reported. Here we show that MurJ localizes both in the lateral membrane and at midcell, and is recruited to midcell simultaneously with late-localizing divisome proteins and proteins MraY and MurG. MurJ septal localization is dependent on the presence of a complete and active divisome, lipid II synthesis and PBP3/FtsW activities. Inactivation of MurJ, either directly by mutation or through binding with MTSES, did not affect the midcell localization of MurJ. Our study visualizes MurJ localization *in vivo* and reveals a possible mechanism of how MurJ functions during cell division, which gives possibilities for future investigations and further antibiotics developments.

Key words: peptidoglycan synthesis, lipid II, flippase, divisome, *E. coli*

Introduction

Rod-shaped bacteria such as the Gram-negative bacterium *Escherichia coli* grow by elongation and binary fission. One of the requirements for proliferation is the enlargement of their cell envelope, which contains an inner membrane (IM) and an outer membrane (OM). The shape of the bacterium is determined by the shape of its peptidoglycan (PG) layer, which is attached to the outer membrane in the periplasmic space located between both membranes of the envelope (Vollmer, Blanot, & De Pedro, 2008). The PG layer is a mesh-like heteropolymeric macromolecule of alternating *N*-acetylmuramyl-peptides (MurNAc-pentapeptides) and *N*-acetylglucosamine (GlcNAc) disaccharides that are connected by a β-(1,4) bond forming glycan chains that are crosslinked between *meso* diaminopimelic acid (DAP) and D-Ala at the third and fourth position of the acceptor and donor stem peptide, respectively (Bouhss, Trunkfield, Bugg, & Mengin-Lecreulx, 2008). The biosynthesis of PG is a complicated process that can be divided into 3 stages. In the cytoplasmic stage, the nucleotide precursors UDP-GlcNAc and UDP-MurNAc-pentapeptide are synthesized from fructose-6-phosphate by the GlmSMU and MurABCDEF proteins, respectively (Barreteau et al., 2008). In the IM stage, the undecaprenyl-pyrophosphate- (C_{55}) linked intermediates lipid I (C_{55}-MurNAc-pentapeptide) and lipid II (C_{55}-MurNAc(-pentapeptide)-GlcNAc) are formed by the MraY and MurG proteins, respectively (Bouhss et al., 2008). During this stage, lipid II, the building unit of peptidoglycan, is translocated by a "flippase" across the IM (Barreteau et al., 2008; Pomorski & Menon, 2006; Ruiz, 2015, 2016; Scheffers & Tol, 2015). In the periplasmic stage, the MurNAc-pentapeptide-GlcNAc component of lipid II is inserted into the PG layer by the glycosyltransferase and transpeptidase activities of various PBPs (Macheboeuf, Contreras-Martel, Job, Dideberg, & Dessen, 2006; Sauvage, Kerff, Terrak, Ayala, & Charlier, 2008), and the lipoyl moiety C_{55}-PP is cleaved off and recycled (Manat et al., 2014).

In *E. coli,* new PG-building units are inserted into the existing PG layer during length growth by a protein complex termed the elongasome, whereas during division new poles are synthesized from completely new material (Pedro, Quintela, Höltje, & Schwarz, 1997) by proteins that collectively have been termed the divisome (Den Blaauwen, De Pedro, Nguyen-Distèche, & Ayala, 2008). The elongasome is organized by the actin homolog MreB, which localizes underneath the IM in patches

98 in a helix-like distribution. MreB is bound to the membrane by its amphipathic helix,
99 and interacts with the bitopic membrane protein RodZ, the integral membrane
100 proteins MreD and MreC, and the PG synthesis essential proteins RodA and PBP2
101 (Contreras-Martel et al., 2017; Den Blaauwen et al., 2008; Fenton, Mortaji, Lau,
102 Rudner, & Bernhardt, 2016; Morgenstein et al., 2015; van Teeffelen et al., 2011).
103 How the elongasome is regulated is not yet very clear whereas in contrast, cell
104 division has been well investigated. During cell division, at least 20 proteins are
105 recruited to midcell to form the divisome. The tubulin homologue FtsZ is attached to
106 the IM at midcell by the anchor proteins FtsA and ZipA, and polymerizes to form the
107 Z-ring (Blaauwen, Buddelmeijer, Aarsman, Hameete, & Nanninga, 1999; Sun &
108 Margolin, 1998). Simultaneously, other proteins, such as the Zap proteins and FtsEX,
109 are recruited to the ring to form the early divisome or protoring. The protoring then
110 recruits the later divisome proteins FtsK, FtsQ, FtsL, FtsB, FtsW, FtsI (PBP3), PBP1b,
111 FtsN (den Blaauwen, Hamoen, & Levin, 2017), and a number of hydrolases and
112 regulatory proteins (Gray et al., 2015) to form the mature divisome (Aarsman et al.,
113 2005). The arrival of FtsN completes the assembly of the core divisome, and signals
114 to initiate septal PG synthesis (Gerding et al., 2009; Lutkenhaus, 2009; Weiss, 2015).
115 The assembled divisome functions as a scaffold to initiate septal PG synthesis, OM
116 constriction, and the cleavage of the PG layer to separate daughter cells (Gray et al.,
117 2015). Septal PG synthesis is mainly orchestrated by PBP3 and PBP1b (Bertsche et
118 al., 2006; Sauvage et al., 2008), but PBP1a can substitute for PBP1b (Suzuki,
119 Nishimura, & Hirota, 1978; Yousif SY, Broome-Smith JK, 1985). OM constriction is
120 organized by the Tol/Pal system, which forms a complex connecting IM and OM
121 (Derouichei, Bénédetti, Lazzaroni, Lazdunski, & Lloubès, 1995; Dubuisson, Vianney,
122 & Lazzaroni, 2002). Tightly controlled amidase activity is involved in the separation
123 of the daughter cells (Priyadarshini, De Pedro, & Young, 2007).
124 Although the stages of PG synthesis are well understood, conflicting
125 information on the flipping of lipid II across the IM has been published over the last
126 few years. In *E. coli*, RodA and FtsW that belong to the SEDS (shape, elongation,
127 division, sporulation) family, and MurJ that belongs to the MOP (multidrug/oligo-
128 saccharidyl-lipid/polysaccharide) export super family (Ruiz, 2008), are reported as
129 candidates of lipid II flippase, either functioning in elongation or division only or in
130 both (Ikeda et al., 1989; Ruiz, 2015; Young, 2014). An alternative activity as
131 glycosyltransferase was recently reported for RodA in *Bacillus subtilis* (Meeske et al.,

2016), while the debate which protein is responsible for lipid II flipping is still going on. FtsW is an essential integral membrane cell division protein with 10 trans-membrane helixes (TMHs) and is conserved in most bacterial species that have a PG cell wall (Khattar, Begg, & Donachie, 1994). FtsW, PBP3 and PBP1b form a complex that is recruited to midcell at the later stage of divisome assembly (Goehring, Gonzalez, & Beckwith, 2006; Goehring, Gueiros-filho, & Beckwith, 2005; Leclercq et al., 2017). FtsW was shown *in vitro* to have lipid II binding and flipping activity, for which two charged residues in TMH 4, arginine 145 and lysine 153, appeared to be essential (Leclercq et al., 2017; Mohammadi et al., 2011, 2014).

MurJ is an essential IM protein that contains 14 TMHs with both C- and N-termini in the cytoplasm (Butler, Davis, Bari, Nicholson, & Ruiz, 2013; Butler, Tan, Joseph, & Ruiz, 2014). Depletion of MurJ will cause irregularly shaped cell, and finally result into cell lysis (Ruiz, 2008). Earlier functional and structural studies of MurJ reveal an outward-facing central cavity that is formed by TMHs 1, 2, 7 and 8, which contain several charged residues that are essential for MurJ function (Butler et al., 2013, 2014), while the observation of an open inward-facing conformation in the crystal structure of MurJ from *Thermosipho africanus* ($MurJ_{TA}$) suggests alternative conformational changes of MurJ (Kuk, Mashalidis, & Lee, 2017). *In vivo* evidence favors MurJ over FtsW as the lipid II flippase, and depletion or inhibition of MurJ caused the accumulation of lipid II in cells (Qiao et al., 2017; Ruiz, 2008; Sham et al., 2014; Young, 2014), while *in vitro* flipping activity has thus far only be established for FtsW (Mohammadi et al., 2011, 2014). Interestingly, the function of MurJ in *E. coli* can be replaced by other flippases that lack sequence similarity, such as the O-antigen flippase Wzk from *E. coli*, and Amj and YtgP from other species (Elhenawy et al., 2016; Hong, Liu, & Reeves, 2018; Meeske et al., 2015; Ruiz, 2009). Two *in vitro* studies on lipid II binding of MurJ showed conflicting results, as one reported a higher lipid II binding affinity of MurJ compared with FtsW (Bolla et al., 2018), while the other one showed lipid II binding only by FtsW but not by MurJ (Leclercq et al., 2017). Although these data support MurJ to be involved in flipping lipid II, it is still not clear where and how MurJ functions in bacterial cells. In this study, by visualizing the cellular localization of MurJ with functional fluorescent protein fusions, we provide new evidence on how MurJ performs its function during PG synthesis.

166 **Results**

167 **Construct a functional fluorescent protein fusion to the N-terminus of MurJ**. To
168 investigate the MurJ function and localization *in vivo*, fluorescent protein (FP) fusions
169 to either the N-terminus or the C-terminus of MurJ with different repeats of Gly-Gly-
170 Ser (GGS) linkers were constructed (X. Chen, Zaro, & Shen, 2013). Two low-copy-
171 number plasmids, pTHV037 and pSAV057, were used to express the fused proteins
172 under the control of a down-regulated $P_{trcdown}$ promoter (van der Ploeg, Goudelis, &
173 den Blaauwen, 2015). Based on the physical properties of fluorescent proteins
174 (Cranfill et al., 2016; Meiresonne, van der Ploeg, Hink, & den Blaauwen, 2017),
175 green fluorescent protein mNeonGreen (mNG) and red fluorescent protein mCherry
176 (mCh) were chosen for MurJ fusions. The functionality of the MurJ fusions was
177 tested by a complementation assay (Material and Methods).

178 As shown in Table 1, the N-terminal fusions of MurJ were fully functional,
179 while C-terminal fusions were less functional or not functional at all. Among these,
180 the N-terminal mNG fusion with a $(GGS)_2$ linker showed the most stable and
181 strongest fluorescence signals. For mCh, the fusion without linker was the best. Thus
182 they were chosen for further studies. The crystal structure of MurJ from *T. africanus*
183 reveals that TMHs 13 and 14 form a hydrophobic groove, which penetrates into the
184 central transport cavity and is hypothesized to be important for lipid II binding (Kuk
185 et al., 2017). The loss function of MurJ C-terminal fusions might due to the defects in
186 folding and groove formation.

187

188 **MurJ localizes in the lateral wall and also at midcell**. MurJ is reported to be
189 present at 674 and 78 molecules per cell when grown in rich and minimal medium,
190 respectively (Li, Burkhardt, Gross, & Weissman, 2014). In order to characterize MurJ
191 at its endogenous expression level, the MurJ fusion was introduced into the *E. coli*
192 chromosome at its native locus. The existence of the native promoter p_{murJ} was
193 confirmed by inserting a divergently transcribed chloramphenicol cassette between
194 the stop codon of gene *yceM* upstream of *murJ* and the putative *murJ* promoter (Fig.
195 S1A). However, attempts to introduce FP-fused MurJ under the native *murJ* promoter
196 failed, apart from a mCh fusion, which yielded a strain with defects in cell
197 morphology and growth (Fig. S1B). Since the plasmid expressed fusions were fully
198 functional, a likely explanation for the morphological defect could be that the

199 translation efficiency of the fused proteins was less than that of MurJ only.
200 Consequently, the expression of the FP fused MurJ under the native *murJ* promoter
201 was not enough to support growth. Therefore, we replaced the chromosomal *murJ*
202 gene with *fp-murJ* constructs transcribed under the control of $p_{trcdown}$ promoter to
203 generate strains XL08 and XL09 (Material and Methods). No defect on growth or cell
204 morphology was observed even when grown without IPTG induction (Fig. S1 C and
205 D).
206 Strain XL08 was grown to steady state in minimal glucose medium (Gb1) at
207 28°C to be able to correlate its length to its cell division cycle age (Blaauwen et al.,
208 1999; Vischer et al., 2015), and the localization of MurJ in living *E. coli* cells was
209 analyzed using ImageJ and the Coli-Inspector of ObjectJ (Vischer et al., 2015). To
210 avoid overexpression, no IPTG induction was applied. The mass double time (MD) of
211 this strain is 83 minutes, which is close to 80 minutes of wild-type *E. coli* (Vischer et
212 al., 2015). MurJ localized in the cylindrical part of the cells as well as specifically at
213 midcell in dividing cells (Fig. 1). After normalizing and plotting the fluorescence
214 profiles into 10 age groups, a clear midcell localization was observed starting from
215 50% of the cell cycle. The septal proportion of MurJ, which is indicated as the "Ring
216 fraction", was analyzed as function of the division cell cycle, and a maximal
217 proportion of 8.58% was observed at 82.5% of cell cycle (Fig. S2). To show that this
218 accumulation was not an effect of double membrane formation during cell
219 invagination, the localization of mNG-$(GGS)_2$-GlpT was introduced as control. GlpT
220 (glycerol-3-phosphate transporter) is the major transporter for the uptake of *sn*-
221 glycerol 3-phosphate in *E. coli*. It was reported to have 12 TMHs and to function as
222 monomer (Huang, 2003), which diffuses homogenously in the IM (Oswald,
223 Varadarajan, Lill, Peterman, & Bollen, 2016). It was therefore expected to show
224 homogenous membrane localization. Like for MurJ, the localization of mNG-$(GGS)_2$-
225 GlpT was imaged and analyzed. As expected, GlpT localized homogenously in the
226 membrane without midcell accumulation. After plotting into 10 age groups, GlpT
227 showed a clear difference with MurJ, and no enhanced fluorescence was observed at
228 midcell during constriction (Fig. 1A and B). The differences between the localization
229 patterns of the two proteins are also obvious in images of the cells (Fig. 1C). The
230 specific localization pattern of MurJ suggests that MurJ is likely involved in both
231 length growth and cell division.
232

233 **MurJ is recruited to midcell simultaneously with the PG synthesis proteins.**
234 The observation of MurJ midcell localization prompted us to the next question: at
235 which point of the cell division cycle MurJ is recruited. To reveal this, localization of
236 MurJ, the early and late localizing proteins FtsZ and FtsN, respectively, and the
237 proteins MraY and MurG, which synthesize Lipid I and lipid II, respectively
238 (Aarsman et al., 2005; Bisson Filho et al., 2017; Bouhss, Mengin-Lecreulx, Le Beller,
239 & Van Heijenoort, 1999; Mengin-Lecreulx, Texier, Rousseau, & Van Heijenoort,
240 1991; Mohammadi et al., 2007; Weiss, 2015) was determined in steady-state grown
241 strain XL08. Cells from the same culture and optical density were either imaged live
242 for MurJ localization or were fixed with FAGA (2.8% formaldehyde and 0.04%
243 glutaraldehyde) and subsequently immunolabeled with antibodies specific for the
244 above mentioned proteins (Buddelmeijer, Aarsman, & Blaauwen, 2013). The early
245 divisome protein FtsZ was recruited at midcell at about 25% of cell cycle, and the
246 core divisome assembly was completed by the midcell arrival of FtsN at 40%-50% of
247 the cell division cycle (Fig.2). The measured extra fluorescence at mid cell (FCplus)
248 of these proteins plotted as function of the cell division cycle age (Fig. S3) is in
249 agreement with a previous study (Van der Ploeg et al., 2013). Interestingly, MraY,
250 MurG and MurJ accumulated at midcell simultaneously at approximately 50% of cell
251 cycle at the later stage of divisome assembly. These results indicate that MurJ is very
252 likely functioning together with the PG synthesis complex, which would be in
253 agreement with its function as a lipid II flippase.
254
255 **MurJ requires a mature divisome for midcell localization**. The timing of MurJ
256 midcell localization raised the question whether its localization is dependent on
257 particular divisome proteins. To answer this, the mNG-$(GGS)_2$-MurJ chromosomal
258 fusion was introduced into a series of temperature-sensitive cell division mutant
259 strains. FtsA is an essential early divisome protein that anchors the Z-ring to the IM
260 (Pichoff & Lutkenhaus, 2005; Rico, García-Ovalle, Mingorance, & Vicente, 2004).
261 The absence of FtsA causes filamentous growth of *E. coli*, as the downstream
262 divisome proteins are not recruited to midcell (Pichoff & Lutkenhaus, 2002). In the
263 FtsA(*Ts*) background, MurJ showed normal midcell localization when grown at
264 permissive temperature. However, when grown at 42 °C, MurJ midcell localization
265 was lost, and MurJ only localized in the cylindrical membrane of the filamentous cells

266 (Fig. 3B and Fig. S4). This indicates that MurJ midcell localization is dependent on
267 the presence of the early divisome. Like in the FtsA(*Ts*) cells, depletion of the later
268 divisome proteins, FtsQ, FtsW, FtsI or FtsN (Ishino et al., 1989; Taschner, Huls, Pas,
269 & Woldringh, 1988), abolished MurJ midcell localization in the filamentous cells
270 (Fig. 3 C-F, and Fig. S4). To point out, some localization bands of MurJ were
271 observed in FtsQ(*Ts*) filaments at 42 °C, which was likely caused by the
272 relocalization of FtsQ proteins during the imaging at room temperature. As control,
273 MurJ still localized at midcell in a wild-type background at 42 °C (Fig. 3A). These
274 results suggest that MurJ requires a mature divisome for midcell localization. To
275 determine to what extent MurJ is dependent on cell division, we also examined MurJ
276 localization in strains that were deleted for PBP1a, PBP1b, Pal, TolA, or the amidases
277 AmiABC. The observation of a clear MurJ midcell localization in the absence of
278 these proteins, even when cells grow as chains, indicates that MurJ midcell
279 localization is independent of these proteins (Fig. 3 G-K). All these results are
280 consistent with the function of MurJ as the lipid II flippase during PG synthesis.
281
282 **MurJ midcell localization requires PBP3 activity**. After observation of MurJ
283 midcell localization, the next obvious question would be whether this localization is
284 dependent on septal PG synthesis. Septal PG synthesis requires the activity of PBP3
285 (FtsI) and PBP1b, although the latter can be replaced by PBP1a (Yousif SY, Broome-
286 Smith JK, 1985). The specific inhibition of PBP3 activity by aztreonam blocks septal
287 PG synthesis without initially inhibiting the localization of the divisome, resulting in
288 filamentous cells with divisomes localized at regular cell division distances (Den
289 Blaauwen, Aarsman, Vischer, & Nanninga, 2003; Mohammadi et al., 2007). After
290 growing the chromosomal mNG-MurJ containing strain XL08 at 28 °C to steady state
291 in Gb1 medium, MurJ localization was determined in the presence of 1 $mg.L^{-1}$
292 aztreonam. A block of MurJ midcell localization was already observed after 30 min,
293 without much change in cell morphology (Fig. S5). After 1 MD and 2 MDs, MurJ
294 midcell localization was completely abolished in the typical filamentous cells (Fig. S5
295 and Fig. 4). Subsequently, cells were fixed and immunolabeled with antibodies
296 against FtsZ and FtsN to show the localization of divisomes, and against MraY and
297 MurG to show the localization of the lipid II-synthesizing complex. As expected, we
298 found that FtsZ, FtsN, MurG and MraY localized at potential division sites in the

filaments (Fig. 4). Likewise, MurJ localization was determined in the presence of elongasome inhibitors A22 and mecillinam for 2 MDs, which inactivate MreB and PBP2, respectively (Den Blaauwen et al., 2003; Shih, Kawagishi, & Rothfield, 2005; Vollmer et al., 2005; White & Gober, 2012). No influence on MurJ midcell localization was observed although cells started to grow spherically (Fig. S6). Together, these results suggest that MurJ localization is specifically dependent on the activity of PBP3 and septal PG synthesis.

MurJ midcell localization requires lipid II synthesis. Next, we asked whether MurJ localization would be lipid II-dependent. The biosynthesis of lipid II requires the activity of two essential enzymes in the cytoplasmic stage, the pyridoxal 5'-phosphate (PLP) dependent alanine racemase, Alr, which converts L-alanine into D-alanine (Barreteau et al., 2008; Wood & Gunsalusa, 1959), and the ATP-dependent D-ala:D-ala ligase, Ddl, which catalyzes the formation of D-alanyl-D-alanine from two molecules of D-alanine (Barreteau et al., 2008; Neuhaus, 1962). D-cycloserine (DCS) is a structural analogue of D-alanine that inactivates Alr and Ddl, and causes rapid cell lysis (Azam & Jayaram, 2015; Neuhaus & Lynch, 1972; Prosser & de Carvalho, 2013; Wang, Walsh, & Walsh, 1978). A concentration of 1 $\mu g.ml^{-1}$ DCS is sufficient to deplete the UDP-MurNac-pentapeptide pool in 30 minutes when *E. coli* is grown in minimal medium (de Roubin, Mengin-Lecreulx, & van Heijenoort, 1992; Mengin-lecreulx et al., 1983). Therefore, steady-state grown XL08 cells were treated with different concentrations of DCS, and MurJ localization was determined at 30 min after adding DCS. At concentrations of 0.5 $\mu g.mL^{-1}$ DCS or higher, growth inhibition and rapid cell lysis was observed after 30 min, while lower concentrations of DCS caused lysis after 1 MD or even longer incubation periods (Fig. 5A). Interestingly, DCS also showed a concentration-dependent effect on MurJ localization. Increasing DCS concentrations eventually blocked the MurJ midcell localization, and when the DCS concentration was higher than 0.5 $\mu g.mL^{-1}$, MurJ was mostly absent from midcell (Fig. 5B and Fig. S7A). In addition, localization of MraY and MurG was somewhat reduces at midcell in the presence of DCS (Fig. S7, B and C). On the contrary, the core divisome monitored by the presence of FtsN remained intact (Fig. S7D). Together, these results indicate that MurJ midcell localization is dependent on the synthesis of lipid II.

333 **MurJ midcell localization requires FtsW activity**. Our results so far showed that
334 MurJ midcell localization is dependent on the assembly of the divisome, the activity
335 of PBP3 and also the synthesis of lipid II. Previous investigation of divisome
336 assembly and regulation suggests that FtsQLB normally keeps FtsW/PBP3 inactive,
337 and once the divisome is completely assembled, the FtsW/PBP3 complex is somehow
338 activated (Liu, Persons, Lee, & de Boer, 2015; Weiss, 2015). Very recently, *in vitro*
339 data showed that FtsW, PBP3 and PBP1b form a ternary complex, and the lipid II
340 binding activity of FtsW inhibits the polymerization of lipid II by PBP1b in the
341 absence of PBP3, while the presence of PBP3 stimulates the release of lipid II from
342 FtsW, and activates its polymerization by PBP1b (Leclercq et al., 2017). These
343 observations raised the possibility that FtsW is needed to ensure the lipid II
344 accessibility to MurJ, which implied that MurJ would not be able to localize at
345 midcell in the presence of inactive FtsW. To validate this hypothesis, plasmids that
346 expressed two non-functional FtsW mutants, FtsW R145A and FtsW K153N were
347 introduced into strain XL08 to investigate the localization of MurJ. These two
348 mutants were shown to localize at midcell but failed to complement the FtsW(*Ts*)
349 strain at non-permissive temperature, and their expression in LMC500 wild-type cells
350 showed a dominant-negative filamentous morphology (Mohammadi et al., 2014). In
351 addition, *in vitro* data showed that these mutants lost the lipid II "flipping" activity of
352 FtsW (Mohammadi et al., 2014). In our study, to eliminate the role of the wild-type
353 FtsW, 20 μM IPTG was used to overexpress these two mutants, and thus diluted the
354 functional wild type FtsW that expressed from the XL08 genome. When cells were
355 grown to steady state in minimal medium, cell length increased due to the defect on
356 cell division, especially in cells expressing mutant K153N (Fig. 6B). MurJ midcell
357 localization was lost in the presence of non-functional FtsW mutants for 2 MDs,
358 despite the overexpression of MurJ as it is also expressed under the IPTG inducible
359 $P_{trcdown}$ promoter. In contrast, the divisome, which was monitored by immunolabeling
360 of FtsN, was still localized at midcell (Fig. 6). Midcell localization of MurJ was not
361 affected when wild type FtsW was overexpressed (Fig. S8), indicating that MurJ
362 needs a functional FtsW for its localization at mid cell. Moreover, when grown in LB
363 medium, strains expressing these mutants showed strong defects on morphology and
364 MurJ localization. At early exponential phase (OD_{600} = 0.2), filamentous morphology
365 was observed for all cultures, even for cells grown with glucose that suppressed the
366 expression of the FtsW mutants (Fig. S9A). Interestingly, in cultures at late log phase

367 expressing the FtsW K153N mutant or in cultures at stationary phase expressing the
368 FtsW R145A mutant, some cells started to restore the MurJ localization, especially in
369 the cells that were induced with IPTG (Fig. S9A). Since these mutants are toxic, we
370 wondered whether the XL08 strain lost these FtsW expressing plasmids at high
371 frequency, restoring MurJ localization. A spot assay was carried out to test our
372 hypothesis: cells from each culture were diluted to the same OD_{600} value and spotted
373 on LB and LB-ampicillin agar plates (these two plasmids expressing the FtsW
374 mutants are ampicillin resistant). For both strains, no obvious growth difference was
375 observed on both plates when grown with glucose, indicating that most cells still
376 contained the mutant plasmids. However, for cells that had been induced with IPTG, a
377 large population of cells had lost the FtsW mutant plasmids, as much less growth was
378 observed on the ampicillin plate compared with LB plate (Fig. S9B). These results
379 strongly suggest that MurJ midcell localization requires FtsW activity, rather than its
380 physical presence.
381
382 **MurJ activity is not required for its localization**. Earlier studies revealed several
383 conserved charged residues, R18, R24, R52 and R270 in the central cavity of MurJ
384 that are essential for its function (41–43). To verify whether MurJ needed to be
385 functional to allow midcell localization, an mNG fused MurJ R18A mutant was
386 expressed from plasmid in LMC500. The cells were grown in Gb1 and expression
387 was induced with 20 μM IPTG. As shown in Fig. 7A, the non-functional mutant
388 R18A localized both in the lateral wall and at midcell as was observed for the wild
389 type-MurJ fusion. Although MurJ is likely functional as a monomer based on its
390 structure, the wild-type copy of MurJ from LMC500 genome might still contribute to
391 the localization of this non-functional mutant. To eliminate this potential contribution,
392 localization of the R18A mutant was also determined in strain XL30, a MurJ-
393 depletion strain in which native MurJ production is under an arabinose-inducible
394 promoter (Ruiz, 2008). In the presence of arabinose, no growth defect was observed,
395 and the R18A mutant showed the same localization as in the LMC500 strain (Fig. 7B,
396 left). When grown in the presence of glucose, native MurJ was eventually depleted as
397 morphology defects were observed after 3 hours, however, the mutant R18A was still
398 localized in lateral wall and at midcell (Fig. 7B, right). The localization of the other
399 loss-of-function-mutants showed the same results as R18A (see below). These results
400 suggest that the MurJ function is not required for its localization.

401

402 **MTSES does not influence the localization of MurJ single-cysteine variants**. The
403 function of a number of MurJ single-cysteine mutants, A29C, N49C, S263C and
404 E273C, was reported to be sensitive (only partially in the case of E273C) to MTSES
405 (Butler et al., 2013). MTSES covalently modifies reduced cysteine residues that are
406 exposed to the periplasm. In the absence of MTSES, these mutant proteins are
407 functional, but not when MTSES is bound to their cysteine residues (Chamakura et
408 al., 2017; Qiao et al., 2017; Sham et al., 2014). To investigate whether MTSES affects
409 the functionality of these mutants through the disruption of their recruitment, the
410 localization of their mNG fusions was determined in the presence of MTSES. Having
411 optimized the induction conditions, MurJ cysteine mutants were induced with 40 μM
412 IPTG, and their localization was determined at 10 min and 40 min (20 min for S263C
413 variant due to the higher sensitivity) after addition of 0.5 mM MTSES (Material and
414 Methods and Fig. S10). We found that MTSES influences only the functionality but
415 not the localization of these mutants, as MurJ midcell localization was still observed,
416 in spite of cell lysis after MTSES addition (Fig. 8 A-D, and Fig. S11). As a control,
417 neither the functionality nor localization of cysteine free variant (MurJ Cys^-) was
418 influenced by MTSES (Fig. 8 E).

419 Next, we also investigated whether MTSES influences the localization of the
420 total-loss-of-function mutants, R18C, R24C, R52C, and R270C. Similar MTSES
421 experiments were performed on these mNG-fused mutants in the LMC500
422 background. To eliminate the potential influence of MTSES on wild type MurJ from
423 the LMC500 genome, the MurJ deletion strain expressing mNG fused wild-type MurJ
424 was firstly checked. In agreement with the evidence that the two native cysteine
425 residues in wild-type MurJ are not labeled by MTSES (Butler et al., 2013), no defect
426 on cell growth, morphology or MurJ localization was observed when MTSES was
427 added (Fig. 8F and Fig. S11F). Similarly, no growth or morphology defect was
428 observed after addition of MTSES to the non-functional single cysteine mutants, and
429 MurJ still localized at midcell (Fig. 8G-H, Fig. S11, G-K and Fig. S12). To point out,
430 when induced with 40 μM IPTG, mutant R24C showed strongly reduced fluorescence
431 and a cytoplasmic-like localization, compared to other mutants. However, when
432 induced with 100 μM IPTG, R24C showed a normal MurJ localization and
433 comparable fluorescence, indicating that mutation R24C does not affect MurJ
434 localization (Fig. S12C). Surprisingly, a spontaneous suppressor mutation R447H that

435 is situated at the cytoplasmic end of TMH13 restored fluorescence and showed a
436 typical MurJ localization when induced with 40 μM IPTG (Fig. S7D-F). Since the
437 R24C mutant was reported not to affect protein level (Butler et al., 2014), R24C
438 might slightly change the structure of MurJ, and affect mNG folding and
439 fluorescence, while mutation R447H could somehow suppress this defect.
440 Together, the investigation of MTSES on MurJ cysteine variants supports the
441 notion that MurJ activity is not essential for its localization.
442
443
444 **Discussion**
445 **Recruitment of MurJ to midcell and the coordination of cell division and septal**
446 **PG synthesis**. The synthesis of PG has been studied for decades, and FtsW and RodA
447 have been always considered as the lipid II flippases in elongasome and divisome,
448 respectively (Dai & Lutkenhaus, 1991; Den Blaauwen et al., 2008; Ikeda et al., 1989;
449 Matsuzawa, Hayakawa, Sato, & Imahori, 1973; Mohammadi et al., 2011, 2014;
450 Sieger, Schubert, Donovan, & Bramkamp, 2013). Only recently, MurJ was identified
451 as the lipid II flippase (Elhenawy et al., 2016; Meeske et al., 2015; Qiao et al., 2017;
452 Ruiz, 2008; Sham et al., 2014). FtsW has been shown to bind and flip lipid II and
453 other lipids *in vitro* but not *in vivo* (Mohammadi et al., 2011, 2014), whereas evidence
454 has been provided that MurJ has the lipid II flipping activity *in vivo*, but only lipid II
455 binding activity so far *in vitro* (Bolla et al., 2018; Leclercq et al., 2017; Qiao et al.,
456 2017; Sham et al., 2014). Our study indicates that these observations can be very well
457 all valid, as both FtsW and MurJ are required for lipid II flipping during cell division.
458 Our results show for the first time the specific MurJ cellular localization in *E.*
459 *coli*. Its midcell localization is critically dependent on maturation of the divisome, on
460 PBP3 and FtsW activity, and lipid II synthesis. Interestingly, in *E. coli*, MurJ can be
461 replaced by non-homologous flippases from other organisms (Elhenawy et al., 2016;
462 Fay & Dworkin, 2009; Kuk et al., 2017; Meeske et al., 2015; Ruiz, 2009). Probing the
463 interaction of MurJ with cell division proteins such as PBP3, FtsW, MurG using our
464 cytoplasmic FRET assay (Alexeeva, Gadella, Verheul, Verhoeven, & Den Blaauwen,
465 2010) did not support interaction between these proteins and MurJ, which is also
466 supported by the loss of MurJ localization in aztreonam treated cells that still have an
467 intact divisome at mid cell (Fig. 4). Although negative FRET results are not at all a
468 guarantee for the absence of protein interactions, together with the smoothly

469 replacement of MurJ by other non-homologous flippases, it suggests that protein-
470 protein interactions are likely not involved in MurJ recruitment, which implies that its
471 localization at midcell is driven by its substrate lipid II. This is also in agreement with
472 the delocalization of MurJ in the presence of D-cycloserine that inhibits the
473 production of Lipid-II (Fig. 5). Inactivation of MurJ *In vivo* results in accumulation of
474 lipid II (Qiao et al., 2017; Ruiz, 2008), indicating that lipid II synthesis is independent
475 of the flipping process and MurJ's presence is needed for lipid II translocation but not
476 synthesis. The failure of MurJ to localize at an incomplete divisome or upon
477 inactivation of PBP3 (by aztreonam) or FtsW (by mutation) signifies that lipid II is
478 inaccessible to MurJ under these conditions (Fig 3, 4 and 6).

479 But why would lipid II not be accessible to MurJ under these conditions? One
480 possible explanation could concern the regulation between PBP3 and FtsW to bind
481 lipid II. We showed that MurJ requires FtsW activity for midcell localization. FtsW is
482 clearly able to bind lipid II *in vitro* (Leclercq et al., 2017), and the absence of PBP3
483 causes FtsW to hold lipid II and prevents its polymerization by PBP1b, whereas
484 presence of PBP3 stimulates the release of lipid II from FtsW and allows its
485 polymerization by PBP1b (Leclercq et al., 2017). Adding that an incomplete divisome
486 will keep the FtsW-PBP3 complex activity in check (probably) by the FtsQLB
487 subcomplex (Liu et al., 2015; Weiss, 2015), a logical explanation would be that the
488 inactivated FtsW, either caused by the incomplete divisome assembly, or inactivation
489 of PBP3, or mutations (FtsW R145A and FtsW K513N), is unable to release lipid II to
490 MurJ, and thus blocks MurJ midcell recruitment. An alternative explanation could be
491 that FtsW, stimulated by PBP3, is required to take over the flipped lipid II from MurJ
492 to use it or present it for PG synthesis. The inactivated PBP3 and/or FtsW will keep
493 MurJ from resuming its flipping cycle. In this scenario MurJ would diffuse away from
494 the division site and would provide any available transglycosylase with lipid II.
495 Taking over lipid II from MurJ would be in agreement with the suggested
496 transglycosylase function of FtsW (Meeske et al., 2016). The requirement of
497 FtsW/PBP3 activities would also explain why MurJ is not flipping lipid II *in vitro*. A
498 third possibility, which we cannot exclude presently, is that FtsW and MurJ are both
499 flipping lipid to insert multiple glycan stands simultaneously in the septum as was
500 suggested in the three for one or four for two models of PG insertion during cell
501 division (Egan & Vollmer, 2015).

502 Why would it be necessary to present lipid II at midcell to MurJ (or take it

503 over from MurJ) and does this imply that RodA as an FtsW homolog is also
504 presenting (or taking over) lipid II to/from MurJ during lateral growth? The midcell
505 position is very precisely determined by the cell (Ortiz, Natale, Cueto, & Vicente,
506 2015; Rowlett & Margolin, 2015). If lipid II would be synthesized randomly and
507 flipped randomly, it could lead to loss of precision of the binary fission into identical
508 daughter cells. The observation that inhibition of the elongasome did not affect
509 division or MurJ midcell localization, and the inhibition of the divisome did not
510 influence cell length growth (Fig. 4 and Fig. S6), suggest that lipid II flipping is
511 precisely organized at the position where new PG synthesis should occur. This can be
512 achieved by allowing it only to flip as closely as possible where the substrate is
513 needed, and by only allowing it to bind lipid II next to the proteins that are activated
514 to synthesize the new cell wall.

515 Other studies suggested that MurJ alters between inward-facing and outward-
516 facing conformations during substrate transport (Kuk et al., 2017), and observed that
517 cysteine mutations at the charged residues, R18, R24, R52 and R270, in the cavity
518 center cause the loss function of MurJ, while some other cysteine mutants at position
519 A29, N49, S263 and E273 are functional but not in the presence of cysteine-reactive
520 agent MTSES (Butler et al., 2014; Sham et al., 2014). But how do these residues
521 contribute to the function of MurJ is not clear. Our results show that the functionality
522 of MurJ is not required for its midcell recruitment, despite the inactivation caused
523 directly by mutation or by MTSES treatment (Fig. 7 and 8). As we mentioned above,
524 MurJ midcell recruitment is likely driven by its substrate lipid II, our results on the
525 MurJ mutants suggest that these mutants are able to recognize at least part of the
526 substrate lipid II, but cannot flip. Also, these important residues are not conserved in
527 other flippases that are able to replace MurJ and therefore more likely involved in the
528 flipping mechanism than in initial substrate recognition (Fig. S13).

529 However, residues A29 and S263 are situated at the interface between the two
530 lobes of MurJ, and thus are predicted to be important for MurJ conformational
531 changes from the outward-facing to the inward-facing state, and binding of MTSES at
532 these two positions will trap the protein at the outward-facing state (Kuk et al., 2017;
533 Sham et al., 2014). Also, recent *in vitro* evidence suggests that binding of MTSES at
534 A29C reduced the lipid II binding affinity of MurJ protein (Bolla et al., 2018). This
535 would predict delocalization for the MTSES bound A29C MurJ mutant, whereas we
536 observe the typical midcell localization *in vivo*. If this MTSES bound mutant does not

537 recognize lipid II, its localization would require protein-protein interaction, which is
538 unlikely in view of MurJ's smoothly replacement by completely non-homologous
539 flippases. It would also imply that the dependence of MurJ recruitment on divisome
540 assembly, lipid II synthesis, FtsW activity and PBP3 activity would then be indirect,
541 and that an important unknown factor that determines MurJ localization is missing. *In*
542 *vitro* data are not always completely comparable to the *in vivo* situation, and given the
543 conflicting lipid II binding evidences *in vitro* (Bolla et al., 2018; Leclercq et al., 2017),
544 we assume that the MurJ A29C MTSES mutant still has a partial ability to recognize
545 lipid II. According to the present published models (Chamakura et al., 2017; Kuk et
546 al., 2017; Qiao et al., 2017), this would require changing to the inward open
547 conformation, which is the only conformation observed thus far in MurJ crystals (Kuk
548 et al., 2017).
549
550 **Model of MurJ function in septal PG synthesis**. Based on our evidence and that of
551 others (23, 38, 39, 41, 43, 44, 90, 91), we arrived at a model for the mechanism of
552 MurJ recruitment and lipid II flipping during septal PG synthesis (Fig. 9). After
553 maturation of the core divisome complex, MurJ is recruited to midcell through the
554 recognition of its substrate lipid II (Fig. 9 A), and ensures the precise positioning of
555 septal PG synthesis. Interruption of lipid II synthesis by D-cycloserine, or inactivation
556 of PBP3 by aztreonam, or inactivation of FtsW will likely make lipid II inaccessible
557 for MurJ, and block the recruitment of MurJ to midcell. Once recruited, MurJ flips
558 lipid II by changing from the inward-facing state to an outward-facing conformation,
559 and the flipped lipid II can be used for new PG synthesis (Fig. 9 B and C).
560 Subsequently, the unloaded outward facing MurJ switches back to the inward-facing
561 state, and can be recruited for new cycles (Fig. 9D). Inactivation of MurJ, either by
562 direct mutation at the charged residues R18, R24, R52, R270, or by binding of
563 MTSES to residues A29C, N49C, S263C and E273C, will disrupt the translocation of
564 lipid II across the membrane (Fig. 9B). Although we cannot totally rule out the
565 possibility of involvement of protein-protein interaction recruitment of MurJ during
566 septal PG synthesis, our data show a possible mechanism of how MurJ functions
567 during cell division *in vivo*, and visualize of MurJ localization will give possibilities
568 for future investigations and further antibiotics developments. It should be noted that
569 although we mainly focused on the septal MurJ, some evidence, like the D-
570 cycloserine experiments, MurJ depletion experiment, and MTSES experiments,

571 showed a global effect on *E. coli*, indicating that MurJ very likely works similarly in
572 collaboration with the elongasome, likely with the FtsW homologous protein RodA.
573
574 **Material and methods**
575
576 **Strains and plasmids construction**
577 Strains and plasmids used in this study are listed in Table. S1. To construct the MurJ
578 N-terminal fluorescent protein (FP) fusion plasmids, mCherry (mCh) (Cranfill et al.,
579 2016) or *E. coli* codon optimized mNeonGreen mNG (Meiresonne et al., 2017), were
580 firstly cloned into plasmids pTHV037 (Den Blaauwen et al., 2003) and pSAV057
581 (Alexeeva et al., 2010) by restriction and ligation (*Nco*I and *Eco*RI), to generate
582 plasmid pSAV047 and pSAV057-mNG, respectively. Subsequently, amplified MurJ
583 fragments with different linkers were cloned into these two plasmids by restriction
584 and ligation (*Eco*RI and *Hind*III), to generate the derived N-terminal fusion plasmids.
585 To construct the MurJ C-terminal FP fusion plasmids, MurJ gene was firstly cloned
586 into plasmids pTHV037 and pSAV057 with *Nco*I and *Bam*HI, to generate plasmids
587 pXL09 and pXL10. Subsequently, FP genes with different linkers were cloned into
588 these two plasmids with *Bam*HI and *Hind*III, to generate the derived C-terminal
589 fusion plasmids. GlpT fusion plasmid pXL28 was constructed in the same way. To
590 construct the MurJ mutant plasmids, QuickChange site directed mutagenesis (Agilent
591 technologies, Santa Clara, CA) and Gibson assembly (Gibson et al., 2009) approaches
592 were applied. Plasmid pXL74 was firstly generated from pXL05 by replacing the wild
593 type MurJ with the cysteine free mutant that was amplified from plasmid
594 pFLAGMurJΔCys (Butler et al., 2013). Single-cysteine-mutant plasmids were
595 constructed afterwards by replacing the original residues with cysteine. The double
596 mutation plasmid pXL93 was constructed by introducing the additional R52C
597 mutation into plasmid pXL82.
598
599 The MurJ deletion strain XL03 (LMC500 Δ*murJ*::FRT/pRC7MurJKan) was
600 constructed by λ-Red recombination (Datsenko & Wanner, 2000) in the presence of
601 the complementing plasmid pRC7MurJ (Butler et al., 2013). Primers priXL17 and
602 priXL18 were used to amplify the MurJ upstream homologous sequence region ahead
603 of MurJ start codon from the *E. coli* genome, primers priXL19 and priXL20 were
604 used to amplify the chloramphenicol (cat) cassette from plasmid pKD3(Datsenko &

605 Wanner, 2000), and primers priXL21 and priXL22 were used to amplify the
606 downstream homologous sequence that comes after MurJ stop codon from the *E. coli*
607 genome. An overlap PCR was performed using the obtained homologous sequences
608 and *cat* gene with primers priXL17 and priXL21 to generate the final recombination
609 fragment. This PCR product was used to generate the MurJ depletion strain sNM01
610 (LMC500 ΔmurJ::cat pRC7MurJKan). Subsequently, the chloramphenicol resistance
611 cassette was removed by plasmid pCP20 (Datsenko & Wanner, 2000), which resulted
612 in the final *murJ* deletion strain XL03/pRC7MurJΔKan (The kanamycin cassette on
613 this plasmid is also removable).
614
615 To prove the existence of the native *murJ* promoter, a chloramphenicol cassette was
616 inserted after the stop codon of *yceM* upstream of *murJ* with a similar strategy as
617 above. Primers priXL49 and priXL50 were used to amplify the upstream homologous
618 sequence from the *E. coli* genome, priXL54 and priXL52 were used to amplify the cat
619 cassette from plasmid pKD3, and priXL45 and priXL48 were used to amplify the
620 downstream homologous sequence from the *E. coli* genome. The amplified overlap
621 PCR product with primers priXL49 and priXL48 was used to construct the
622 recombinant strain XL04 that interrupted MurJ expression from the upstream gene
623 cluster. To construct MurJ chromosomal fusion strains that are expressed under its
624 native promoter, plasmids pXL36 and pXL37 were firstly constructed with Gibson
625 assembly: primers priXL51 and priXL52 were used to amplify the pKD3 backbone,
626 primers priXL45 and priXL46 were used to amplify the P_{murj} sequence from the *E.*
627 *coli* genome, primers priXL53 and priXL47 were used to amplify FPs-MurJ sequence
628 from plasmid pXL05 and pNM037. The final recombination fragments were
629 generated by overlap PCR of 2 fragments with primers priXL17 and priXL48 from
630 fragment *yceM-cat* amplified from the XL04 genome with primers priXL17 and
631 priXL50, and fragment *cat-*P_{murj}*-FPs-murJ* amplified from these assembled plasmids
632 with primers priXL54 and priXL48. To construct the MurJ chromosomal FP fusion
633 strains XL06 and XL07 expressing MurJ under control of the $P_{trcdown}$ promoter,
634 fragment *yceM-cat* was amplified from the XL04 genome with primers priXL17 and
635 priXL52, and fragment $P_{trcdown}$*-FPs-MurJ* was amplified from plasmids pXL06 or
636 pNM037 with primers priXL77 and priXL48. The two fragments were used for an
637 overlap PCR with primers priXL17 and priXL48 and the resulting sequence was used
638 to construct strains XL06 and XL07 from LMC500 by λ-Red recombination. To insert

639 the mNG-MurJ fusion in the chromosomal of temperature sensitive strains and
640 deletion strains, PCR fragment *yceM-cat-*$P_{trcdown}$*-NG-(GGS)*$_2$*-MurJ* was firstly
641 amplified from the XL06 genome with primer priXL17 and priXL48, and
642 subsequently introduced into other strains by λ-Red recombination.
643 To construct an FtsN depletion strain, primers priXL140 and priXL141 were used to
644 amplify the upstream sequence of FtsN from the *E. coli* genome, priXL54 and
645 priXL52 were used to amplify the *cat* cassette from plasmid pKD3, and priXL138 and
646 priXL139 were used to amplify the *araC-*P_{BAD} region from plasmid pJC83 (J. C.
647 Chen & Beckwith, 2008). An overlap PCR with priXL140 and priXL138 was
648 performed subsequently to generate the final product for recombination. The MurJ
649 depletion strain was constructed in a similar way, primers priXL17 and priXL52 were
650 used to amplify the *YceM-cat* region from the XL06 genome, priXL126 and priXL157
651 were used to amplify *araC-*P_{BAD} region from plasmid pKD46, priXL156 and priXL48
652 were used to amplify the MurJ region from the *E. coli* genome. The final PCR product
653 for MurJ depletion was generated by an overlap PCR with primers priXL17 and
654 priXL48.
655
656 All PCR amplifications were performed using the DNA polymerase pfuX7 prepared
657 in our lab as described (Nørholm, 2010), and all restriction enzymes used were
658 purchased from New England Biolabs Inc (NEB, Ipswich, MA).
659
660
661 **Medium and growth conditions**
662 LB medium (10 g of tryptone (Bacto laboratories, Australia), 10 g of NaCl (Merck,
663 Kenilworth, NJ), 5 g of yeast extract (Duchefa, Amsterdam, The Netherlands) per
664 liter) was used for growth in rich medium at 30 °C, 37 °C and 42 °C. The FtsW(*Ts*)
665 strain was grown in LBΔNaCl medium (LB without NaCl and containing 0.1%
666 glucose and 20 mg thymine per liter) as described previously (Pastoret et al., 2004).
667 Gb1 minimal medium (6.33 g of K_2HPO_4 (Merck), 2.95 g of KH_2PO_4 (Riedel de Haen,
668 Seelze, Germany), 1.05 g of $(NH_4)_2SO_4$ (Sigma, St. Louis, MO), 0.10 g of
669 $MgSO_4 \cdot 7H_2O$ (Roth, Karlsruhe, Germany), 0.28 mg of $FeSO_4 \cdot 7H_2O$ (Sigma), 7.1 mg
670 of $Ca(NO_3)_2 \cdot 4H_2O$ (Sigma), 4 mg of thiamine (Sigma), 2 mg of uracil (Sigma), 2 mg
671 of lysine (Sigma), 2 mg of thymine (Sigma), and 0.5 % glucose (Merck) per liter, pH
672 7.0) was prepared for steady state growth at 28 °C as described (Van der Ploeg et al.,

673 2013). Protein expression was induced with isopropyl β-D-1-thiogalactopyranoside
674 (IPTG, Promega, Madison WI) or L-(+)arabinose (Sigma) at described
675 concentrations. All antibiotics were purchased from Sigma Aldric, Working
676 antibiotics concentrations were: 100 μg.mL^{-1} ampicillin (10 μg.mL^{-1} for Δ*tolA* and
677 Δ*pal* strains), 25 μg.mL^{-1} chloramphenicol, 50 μg.mL^{-1} kanamycin, 10 μg.mL^{-1}
678 tetracycline (for chromosomal recombinant strains, half of the concentrations were
679 used). Optical density (OD) was measured at 450 nm and 600 nm when grown in
680 minimal medium and rich medium, respectively.
681
682 **Testing functionality of MurJ fusions**
683 Functionality experiments were performed as described previously (Butler et al.,
684 2013, 2014) using the MurJ depletion strain XL03 that expresses a functional MurJ
685 copy from plasmid pRC7MurJΔKan. This plasmid has partitioning defects causing
686 some of the daughter cells to lose this plasmid and die after division, unless they are
687 complemented with a functional copy of MurJ since MurJ is essential for *E. coli*. In
688 addition, pRC7MurJΔKan contains the *lac*Z operon and thus cells that lost the
689 plasmid will also lose their ability to produce the blue color on 20 μg.L^{-1} X-gal
690 (Sigma) agar plates, as our pTHV and pSAV-based plasmids do not. The functional
691 FPs fusions to MurJ were obtained by selecting the white colonies on Ampicillin or
692 chloramphenicol X-gal agar dish after transformation. The growth and fluorescence
693 intensity of strains containing a fusion expressing plasmid were investigated with
694 Synergy Mx BioTek plate reader and microscopy.
695
696 **Immunolocalization experiments**
697 *E. coli* cells were fixed with FAGA (2.8% formaldehyde and 0.04% glutaraldehyde
698 final concentration) for 15-20 minutes in a shaking waterbath after steady state
699 growth in Gb1 minimal medium at 28 °C (Den Blaauwen et al., 2003). Subsequently,
700 cells were permeabilized and immunolabeled with antibodies as described
701 (Buddelmeijer et al., 2013). The antibodies against FtsZ, FtsN, MurG used in this
702 study were purified as described (Aarsman et al., 2005; Mohammadi et al., 2007).
703 Polyclonal antibodies against MraY were obtained from Rabbits that were injected
704 with an antigenic peptide that was designed with the Epiros program (Biosiris).
705 Based on the predicted topology by Bouhss et al (16,17) the peptide localizes in the
706 cytoplasmic loop between TMH 1 and 2. The sequence was H2N-

707 G54QVVRNDGPESHFS67C-COOH. The cysteine was added at the C-terminal to
708 perform the coupling with the KLH carrier protein.
709
710 **Depletion or inactivation of of divisome proteins**
711 Strain XL17, XL15, XL13 and XL14 that contain a MurJ FP fusion and the
712 temperature sensitive divisome mutant proteins FtsW, FtsI, FtsQ and FtsA,
713 respectively, were diluted 1:1000 from overnight cultures (grown at 30 °C) into fresh
714 LB medium (LB Δ NaCl medium for XL13) with 12.5 μg.mL^{-1} chloramphenicol, and
715 grown at 30 °C to OD_{600} of approximately 0.2. Cells were diluted 1:5 into the same
716 fresh medium that was pre-warmed at 30 °C and 42 °C, respectively, and kept
717 growing for 2 mass doublings. To deplete FtsN, strain XL23 was diluted 1:1000 from
718 an overnight culture (grown at 30 °C) into fresh LB medium with 12.5 μg.mL^{-1}
719 chloramphenicol and 0.5% w/v glucose, and kept growing at 30 °C to OD_{600} of
720 approximately 0.2. Induced with 0.2% w/v arabinose was set as control. After growth,
721 cells were immobilized on 1% agarose slides, and imaged live by phase contrast and
722 epifluorescence microscopy.
723
724 **MTSES assay**
725 Sodium (2-sulfonatoethyl) methanethiosulfonate (MTSES) was purchased from Santa
726 Cruz Biotechnology Company. A gradient assay on MTSES concentrations (0, 0.01,
727 0.05, 0.1 or 0.5 mg.mL^{-1}) was firstly applied on Gb1 steady state grown strain XL03
728 that expressed the MurJ A29C mutant. MurJ localization was determined by
729 microscopy at 10 min and 40 min after addition of MTSES. Upon induction of
730 expression with 20 μM IPTG for 2 MDs rapid cell lysis was observed after adding
731 MTSES for 10 min at concentrations 0.1mM or 0.5 mM. A pattern of MurJ midcell
732 localization was observed despite the increase of MTSES concentrations (Fig. S7A).
733 However, we noticed that lower concentration of MTSES (0.01 mM) was not
734 sufficient to influence the cell growth, and cells lysed too fast at higher MTSES
735 concentrations (above 0.05 mM) to determine MurJ localization at a longer time scale.
736 Since MTSES targets MurJ A29C by covalent binding, we suspected that the higher
737 expression of MurJ might help to increase the resistance to MTSES. Thus, 40 μM
738 IPTG was used for MurJ induction (2 MDs). Indeed, higher expression of A29C
739 slightly improved the survival of cells, with a yield of better fluorescent signal, and

740 MurJ midcell localization was able to be determined at both 10 min and 40 min after
741 MTSES addition. In addition, 0.5 mM MTSES was sufficient to show the influence
742 on cell growth. Thus, 0.5 mM MTSES and 40 μM IPTG inductions were used for the
743 investigation of MurJ localization in the presence of MTSES.
744
745 **Microscope and image analysis**
746 For localization imaging, cells were immobilized on 1.0% agarose (w/v in Gb1) pads
747 and imaged immediately. Fluorescence microscopy was carried out either with an
748 Olympus BX-60 fluorescence microscope equipped with a CoolSnap *fx*
749 (Photometrics) CCD camera, a 100×/N.A. 1.35 oil objective, and software 'ImageJ-
750 MicroManager', or with a Nikon Eclipse Ti microscope equipped with a C11440-
751 22CU Hamamatsu ORCA camera, a CFI Plan Apochromat DM 100× oil objective, an
752 Intensilight HG 130W lamp and the NIS elements software (version 4.20.01).
753
754 Images were analyzed with Coli-Inspector supported by the ObjectJ plugin for ImageJ
755 (version 1.49v) (Vischer et al., 2015). Briefly, the length and diameter of more than
756 1200 individual cells were marked and analysis in the phase contrast images.
757 Fluorescence and phase contrast images were aligned and fluorescence background
758 was subtracted as described (18). The fluorescence of each cell was collected in a one
759 pixel wide bar with the length of the cell. A map of the diameter or the fluorescence
760 localization and intensity was generated with the cells sorted according to increasing
761 cell from left to right. Because cells were grown to steady state, the length of the cells
762 can be directly correlated to the cell division cycle age. A collective profile is created
763 from all cell profiles in a map. They are first resampled to a normalized cell length of
764 100 data points, and then averaged to a single plot, in either 1 group or more age bins.
765 The FCplus (the extra fluorescence at mid cell in comparison to the fluorescence in
766 the rest of the cell) and Ringfraction (FCplus/Total cellular fluorescence) profiles
767 were generated with the "graph assistant" macro in ObjectJ (18).
768 .
769
770 **ACKNOWLEDGEMENTS.** We would like to thank Dr. N. Ruiz for critically
771 reading the manuscript and for the gift of plasmids pFLAGMurJΔCys and pRC7MurJ
772 for cloning and the functionality testing.
773 X.L. was supported by the Chinese Scholarship Council (File No.201406220123), and

N.Y.M. by NWO ALW open program (822.02.019).

X.L. and T.B. designed most experiments. X.L performed most experiments and N.Y.M designed and performed some of the experiments. X.L and TdB analyzed the data and wrote the manuscript. A.B. isolated MraY and made antibodies against the protein. All authors critically read the manuscript and gave feedback.

References

Aarsman, M. E. G., Piette, A., Fraipont, C., Vinkenvleugel, T. M. F., Nguyen-Distèche, M., & Den Blaauwen, T. (2005). Maturation of the *Escherichia coli* divisome occurs in two steps. *Molecular Microbiology*, *55*(6), 1631–1645. https://doi.org/10.1111/j.1365-2958.2005.04502.x

Al-Dabbagh B, Henry X, El Ghachi M, Auger G, Blanot D, Parquet C, Mengin-Lecreulx D, B. A. (2008). Active Site Mapping of MraY , a Member of the Polyprenyl-phosphate N- Acetylhexosamine 1-Phosphate Transferase Superfamily , Catalyzing the First Membrane Step of Peptidoglycan Biosynthesis †. *Biochemistry*, *47*(34), 8919–8928. https://doi.org/10.1021/bi8006274

Alexeeva, S., Gadella, T. W. J., Verheul, J., Verhoeven, G. S., & Den Blaauwen, T. (2010). Direct interactions of early and late assembling division proteins in *Escherichia coli* cells resolved by FRET. *Molecular Microbiology*, *77*(2), 384–398. https://doi.org/10.1111/j.1365-2958.2010.07211.x

Azam, M. A., & Jayaram, U. (2015). Inhibitors of alanine racemase enzyme: a review. *Journal of Enzyme Inhibition and Medicinal Chemistry*, *6366*(August), 1–10. https://doi.org/10.3109/14756366.2015.1050010

Barreteau, H., Kovač, A., Boniface, A., Sova, M., Gobec, S., & Blanot, D. (2008). Cytoplasmic steps of peptidoglycan biosynthesis. *FEMS Microbiology Reviews*, *32*(2), 168–207. https://doi.org/10.1111/j.1574-6976.2008.00104.x

Bertsche, U., Kast, T., Wolf, B., Fraipont, C., Aarsman, M. E. G., Kannenberg, K., … Vollmer, W. (2006). Interaction between two murein (peptidoglycan) synthases, PBP3 and PBP1B, in *Escherichia coli*. *Molecular Microbiology*, *61*(3), 675–690. https://doi.org/10.1111/j.1365-2958.2006.05280.x

Bisson Filho, A. W., Hsu, Y.-P., Squyres, G., Kuru, E., Wu, F., Jukes, C., … Garner, E. (2017). Treadmilling by FtsZ filaments drives peptidoglycan synthesis and bacterial cell division. *Science*, *355*, 739–743. https://doi.org/DOI: 10.1126/science.aak9973

Blaauwen, T. Den, Buddelmeijer, N., Aarsman, M. E. G., Hameete, C. M., & Nanninga, N. (1999). Timing of FtsZ assembly in *Escherichia coli*. *Journal of Bacteriology*, *181*(17), 5167–5175.

Bolla, J. R., Sauer, J. B., Wu, D., Mehmood, S., Allison, T. M., & Robinson, C. V. (2018). Direct observation of the influence of cardiolipin and antibiotics on lipid II binding to MurJ. *Nature Chemistry*, (January). https://doi.org/10.1038/nchem.2919

Bouhss, A., Mengin-Lecreulx, D., Le Beller, D., & Van Heijenoort, J. (1999). Topological analysis of the MraY protein catalysing the first membrane step of peptidoglycan synthesis. *Molecular Microbiology*, *34*(3), 576–585. https://doi.org/10.1046/j.1365-2958.1999.01623.x

Bouhss, A., Trunkfield, A. E., Bugg, T. D. H., & Mengin-Lecreulx, D. (2008). The

biosynthesis of peptidoglycan lipid-linked intermediates. *FEMS Microbiology Reviews*. https://doi.org/10.1111/j.1574-6976.2007.00089.x

Buddelmeijer, N., Aarsman, M., & Blaauwen, T. den. (2013). Immunolabeling of Proteins in situ in *Escherichia coli* K12 Strains. *Bio-Protocol*, *3*(15), 1–5. https://doi.org/10.21769/BioProtoc.852

Butler, E. K., Davis, R. M., Bari, V., Nicholson, P. A., & Ruiz, N. (2013). Structure-function analysis of MurJ reveals a solvent-exposed cavity containing residues essential for peptidoglycan biogenesis in *Escherichia coli*. *Journal of Bacteriology*, *195*(20), 4639–4649. https://doi.org/10.1128/JB.00731-13

Butler, E. K., Tan, W. B., Joseph, H., & Ruiz, N. (2014). Charge requirements of lipid II flippase activity in *Escherichia coli*. *Journal of Bacteriology*, *196*(23), 4111–4119. https://doi.org/10.1128/JB.02172-14

Chamakura, K. R., Sham, L.-T., Davis, R. M., Min, L., Cho, H., Ruiz, N., … Young, R. (2017). A viral protein antibiotic inhibits lipid II flippase activity. *Nature Microbiology*. https://doi.org/10.1038/s41564-017-0023-4

Chen, J. C., & Beckwith, J. (2008). FtsQ, FtsL and FtsI require FtsK, but not FtsN, for co-localization with FtsZ during *Escherichia coli* cell division. *Molecular Microbiology*. https://doi.org/https://doi.org/10.1046/j.1365-2958.2001.02640.x

Chen, X., Zaro, J. L., & Shen, W. C. (2013). Fusion protein linkers: Property, design and functionality. *Advanced Drug Delivery Reviews*. Elsevier B.V. https://doi.org/10.1016/j.addr.2012.09.039

Contreras-Martel, C., Martins, A., Ecobichon, C., Trindade, D. M., Matteï, P.-J., Hicham, S., … Dessen, A. (2017). Molecular architecture of the PBP2–MreC core bacterial cell wall synthesis complex. *Nature Communications*, *8*(1), 776. https://doi.org/10.1038/s41467-017-00783-2

Cranfill, P. J., Sell, B. R., Baird, M. A., Allen, J. R., Lavagnino, Z., de Gruiter, H. M., … Piston, D. W. (2016). Quantitative assessment of fluorescent proteins. *Nature Methods*, *13*(7), 557–562. https://doi.org/10.1038/nmeth.3891

Dai, K., & Lutkenhaus, J. (1991). *ftsZ* is an essential cell division gene in *Escherichia coli*. *J Bacteriol*, *173*(11), 3500–3506. https://doi.org/10.1046/j.1365-2958.1997.4091773.x

Datsenko, K., & Wanner, B. (2000). One-step inactivation of chromosomal genes in *Escherichia coli* K-12 using PCR products. *Proc. Nat. Acad. Sci. (USA)*, *971242*, 6640–6645. https://doi.org/https://doi.org/10.1073/pnas.120163297

de Roubin, M. R., Mengin-Lecreulx, D., & van Heijenoort, J. (1992). Peptidoglycan biosynthesis in *Escherichia coli*: variations in the metabolism of alanine and D-alanyl-D-alanine. *Journal of General Microbiology*, *138 Pt 8*(1 992), 1751–7. https://doi.org/10.1099/00221287-138-8-1751

Den Blaauwen, T., Aarsman, M. E. G., Vischer, N. O. E., & Nanninga, N. (2003). Penicillin-binding protein PBP2 of *Escherichia coli* localizes preferentially in the lateral wall and at mid-cell in comparison with the old cell pole. *Molecular Microbiology*, *47*(2), 539–547. https://doi.org/10.1046/j.1365-2958.2003.03316.x

Den Blaauwen, T., De Pedro, M. A., Nguyen-Distèche, M., & Ayala, J. A. (2008). Morphogenesis of rod-shaped sacculi. *FEMS Microbiology Reviews*, *32*(2), 321–344. https://doi.org/10.1111/j.1574-6976.2007.00090.x

den Blaauwen, T., Hamoen, L. W., & Levin, P. A. (2017). The divisome at 25: the road ahead. *Current Opinion in Microbiology*, *36*, 85–94. https://doi.org/10.1016/j.mib.2017.01.007

Derouichei, R., Bénédetti, H., Lazzaroni, J. C., Lazdunski, C., & Lloubès, R. (1995).

Protein complex within *Escherichia coli* inner membrane: TolA N-terminal domain interacts with TolQ and TolR proteins. *Journal of Biological Chemistry*, *270*(19), 11078–11084. https://doi.org/10.1074/jbc.270.19.11078

Du, S., Pichoff, S., & Lutkenhaus, J. (2016). FtsEX acts on FtsA to regulate divisome assembly and activity. *Proceedings of the National Academy of Sciences*, 201606656. https://doi.org/10.1073/pnas.1606656113

Dubuisson, J. F., Vianney, A., & Lazzaroni, J. C. (2002). Mutational Analysis of the TolA C-Terminal Domain of *Escherichia coli* and Genetic Evidence for an Interaction between TolA and TolB. *Journal of Bacteriology*, *184*(16), 4620–4625. https://doi.org/10.1128/JB.184.16.4620-4625.2002

Egan, A. J. F., & Vollmer, W. (2015). The stoichiometric divisome: A hypothesis. *Frontiers in Microbiology*, *6*(MAY), 1–6. https://doi.org/10.3389/fmicb.2015.00455

Elhenawy, W., Davis, R. M., Fero, J., Salama, N. R., Felman, M. F., & Ruiz, N. (2016). The o-antigen flippase wzk can substitute for MurJ in peptidoglycan synthesis in *helicobacter pylori* and *Escherichia coli*. *PLoS ONE*, *11*(8), 1–16. https://doi.org/10.1371/journal.pone.0161587

Fay, A., & Dworkin, J. (2009). B*acillus subtilis* homologs of MviN (MurJ), the putative *Escherichia coli* lipid II flippase, are not essential for growth. *Journal of Bacteriology*, *191*(19), 6020–6028. https://doi.org/10.1128/JB.00605-09

Fenton, A. K., Mortaji, L. El, Lau, D. T. C., Rudner, D. Z., & Bernhardt, T. G. (2016). CozE is a member of the MreCD complex that directs cell elongation in *Streptococcus pneumoniae*. *Nature Microbiology*, *2*(December 2016), 16237. https://doi.org/10.1038/nmicrobiol.2016.237

Gerding, M. A., Liu, B., Bendezú, F. O., Hale, C. A., Bernhardt, T. G., & De Boer, P. A. J. (2009). Self-enhanced accumulation of FtsN at division sites and roles for other proteins with a SPOR domain (DamX, DedD, and RlpA) in *Escherichia coli* cell constriction. *Journal of Bacteriology*, *191*(24), 7383–7401. https://doi.org/10.1128/JB.00811-09

Gibson, D. G., Young, L., Chuang, R.-Y., Venter, J. C., Hutchison, C. A., & Smith, H. O. (2009). Enzymatic assembly of DNA molecules up to several hundred kilobases. *Nature Methods*, *6*(5), 343–345. https://doi.org/10.1038/nmeth.1318

Goehring, N. W., Gonzalez, M. D., & Beckwith, J. (2006). Premature targeting of cell division proteins to midcell reveals hierarchies of protein interactions involved in divisome assembly. *Molecular Microbiology*, *61*(1), 33–45. https://doi.org/10.1111/j.1365-2958.2006.05206.x

Goehring, N. W., Gueiros-filho, F., & Beckwith, J. (2005). Premature targeting of a cell division protein to midcell allows dissection of divisome assembly in *Escherichia coli*. *Genes & Development*, *19*(1), 127–137. https://doi.org/10.1101/gad.1253805

Gray, A. N., Egan, A. J. F., van't Veer, I. L., Verheul, J., Colavin, A., Koumoutsi, A., … Vollmer, W. (2015). Coordination of peptidoglycan synthesis and outer membrane constriction during *Escherichia coli* cell division. *eLife*, *4*(MAY), 1–29. https://doi.org/10.7554/eLife.07118

Hong, Y., Liu, M. A., & Reeves, P. R. (2018). Progress in our understanding of Wzx flippase for translocation of bacterial membrane lipid-linked oligosaccharide. *Journal of Bacteriology*, *200*(1), 1–14. https://doi.org/10.1128/JB.00154-17

Huang, Y. (2003). Structure and Mechanism of the Glycerol-3-Phosphate Transporter from *Escherichia coli*. *Science*, *301*(5633), 616–620. https://doi.org/10.1126/science.1087619

921 Ikeda, M., Sato, T., Wachi, M., Jung, H. K., Ishino, F., Kobayashi, Y., & Matsuhashi,
922 M. (1989). Structural similarity among *Escherichia coli* FtsW and RodA proteins
923 and *Bacillus subtilis* SpoVE protein, which function in cell division, cell
924 elongation, and spore formation, respectively. *Journal of Bacteriology*, *171*(11),
925 6375–6378. https://doi.org/10.1128/jb.171.11.6375-6378.1989
926 Ishino, F., Hai Kwan Jung, Ikeda, M., Doi, M., Wachi, M., & Matsuhashi, M. (1989).
927 New mutations *fts-36*, *lts-33*, and *ftsW* clustered in the mra region of the
928 *Escherichia coli* chromosome induce thermosensitive cell growth and division.
929 *Journal of Bacteriology*, *171*(10), 5523–5530.
930 https://doi.org/10.1128/jb.171.10.5523-5530.1989
931 Khattar, M. M., Begg, K. J., & Donachie, W. D. (1994). Identification of FtsW and
932 characterization of a new ftsW division mutant of *Escherichia coli*. *Journal of*
933 *Bacteriology*, *176*(23), 7140–7147. https://doi.org/10.1128/jb.176.23.7140-
934 7147.1994
935 Kuk, A. C. Y., Mashalidis, E. H., & Lee, S. Y. (2017). Crystal structure of the MOP
936 flippase MurJ in an inward-facing conformation. *Nature Structural and*
937 *Molecular Biology*, *24*(2), 171–176. https://doi.org/10.1038/nsmb.3346
938 Leclercq, S., Derouaux, A., Olatunji, S., Fraipont, C., Egan, A. J. F., Vollmer, W., …
939 Terrak, M. (2017). Interplay between Penicillin-binding proteins and SEDS
940 proteins promotes bacterial cell wall synthesis. *Scientific Reports*.
941 https://doi.org/10.1038/srep43306
942 Li, G. W., Burkhardt, D., Gross, C., & Weissman, J. S. (2014). Quantifying absolute
943 protein synthesis rates reveals principles underlying allocation of cellular
944 resources. *Cell*, *157*(3), 624–635. https://doi.org/10.1016/j.cell.2014.02.033
945 Liu, B., Persons, L., Lee, L., & de Boer, P. A. J. (2015). Roles for both FtsA and the
946 FtsBLQ subcomplex in FtsN-stimulated cell constriction in *Escherichia coli*.
947 *Molecular Microbiology*, *95*(6), 945–970. https://doi.org/10.1111/mmi.12906
948 Lutkenhaus, J. (2009). FtsN - Trigger for septation. *Journal of Bacteriology*, *191*(24),
949 7381–7382. https://doi.org/10.1128/JB.01100-09
950 Macheboeuf, P., Contreras-Martel, C., Job, V., Dideberg, O., & Dessen, A. (2006).
951 Penicillin binding proteins: Key players in bacterial cell cycle and drug
952 resistance processes. *FEMS Microbiology Reviews*, *30*(5), 673–691.
953 https://doi.org/10.1111/j.1574-6976.2006.00024.x
954 Manat, G., Roure, S., Auger, R., Bouhss, A., Barreteau, H., Mengin-Lecreulx, D., &
955 Touzé, T. (2014). Deciphering the Metabolism of Undecaprenyl-Phosphate: The
956 Bacterial Cell-Wall Unit Carrier at the Membrane Frontier. *Microbial Drug*
957 *Resistance*, *20*(3), 199–214. https://doi.org/10.1089/mdr.2014.0035
958 Matsuzawa, H., Hayakawa, K., Sato, T., & Imahori, K. (1973). Characterization and
959 genetic analysis of a mutant of *Escherichia coli* K-12 with rounded morphology.
960 *J. Bacteriol.*, *115*(1), 436–442.
961 Meeske, A. J., Riley, E. P., Robins, W. P., Uehara, T., Mekalanos, J. J., Kahne, D., …
962 Rudner, D. Z. (2016). SEDS proteins are a widespread family of bacterial cell
963 wall polymerases. *Nature*, 1–15. https://doi.org/10.1038/nature19331
964 Meeske, A. J., Sham, L.-T., Kimsey, H., Koo, B.-M., Gross, C. a, Bernhardt, T. G., &
965 Rudner, D. Z. (2015). MurJ and a novel lipid II flippase are required for cell wall
966 biogenesis in *Bacillus subtilis*. *Proceedings of the National Academy of Sciences*
967 *of the United States of America*, *112*(20), 6437–42.
968 https://doi.org/10.1073/pnas.1504967112
969 Meiresonne, N. Y., van der Ploeg, R., Hink, M. A., & den Blaauwen, T. (2017).
970 Activity-Related Conformational Changes in d,d-Carboxypeptidases Revealed

971 by In Vivo Periplasmic Förster Resonance Energy Transfer Assay in *Escherichia*
972 *coli*. *mBio*. https://doi.org/10.1128/mBio.01089-17
973 Mengin-lecreulx, D., Flouret, B., Heijenoort, J. V. A. N., S, E. R. C. N. R., Biochimie,
974 I. De, & Paris-sud, U. (1983). Pool Levels of UDP N-Acetylglucosamine and
975 UDP N- Acetylglucosamine-Enolpyruvate in *Escherichia coli* and Correlation
976 with Peptidoglycan Synthesis. *Journal of Bacteriology*, *154*(3), 1284–1290.
977 https://doi.org/0021-9193/83/061284-07$02.00/0
978 Mengin-Lecreulx, D., Texier, L., Rousseau, M., & Van Heijenoort, J. (1991). The
979 murG gene of Escherichia coli codes for the UDP-N-acetylglucosamine:N-
980 acetylmuramyl-(pentapeptide) pyrophosphoryl-undecaprenol N-
981 acetylglucosamine transferase involved in the membrane steps of peptidoglycan
982 synthesis. *Journal of Bacteriology*, *173*(15), 4625–4636.
983 https://doi.org/10.1128/JB.173.15.4625-4636.1991
984 Mohammadi, T., Karczmarek, A., Crouvoisier, M., Bouhss, A., Mengin-Lecreulx, D.,
985 & Den Blaauwen, T. (2007). The essential peptidoglycan glycosyltransferase
986 MurG forms a complex with proteins involved in lateral envelope growth as well
987 as with proteins involved in cell division in *Escherichia coli*. *Molecular*
988 *Microbiology*, *65*(4), 1106–1121. https://doi.org/10.1111/j.1365-
989 2958.2007.05851.x
990 Mohammadi, T., Sijbrandi, R., Lutters, M., Verheul, J., Martin, N. I., Den Blaauwen,
991 T., … Breukink, E. (2014). Specificity of the transport of lipid II by FtsW in
992 *Escherichia coli*. *Journal of Biological Chemistry*, *289*(21), 14707–14718.
993 https://doi.org/10.1074/jbc.M114.557371
994 Mohammadi, T., van Dam, V., Sijbrandi, R., Vernet, T., Zapun, A., Bouhss, A., …
995 Breukink, E. (2011). Identification of FtsW as a transporter of lipid-linked cell
996 wall precursors across the membrane. *The EMBO Journal*, *30*(8), 1425–1432.
997 https://doi.org/10.1038/emboj.2011.61
998 Morgenstein, R. M., Bratton, B. P., Nguyen, J. P., Ouzounov, N., Shaevitz, J. W., &
999 Gitai, Z. (2015). RodZ links MreB to cell wall synthesis to mediate MreB
1000 rotation and robust morphogenesis. *Proc Natl Acad Sci U S A*, *112*(40), 12510–
1001 12515. https://doi.org/10.1073/pnas.1509610112
1002 Neuhaus, F. C. (1962). The enzymatic synthesis of D-alanyl-D-alanine. I. Purification
1003 and properties of D-alanyl-D-alanine synthetase. *Journal of Biological*
1004 *Chemistry*, *237*(3).
1005 Neuhaus, F. C., & Lynch, J. L. (1972). Studies on the inhibition of D-alanyl-D-
1006 alanine synthetase by the antibiotic D-cycloserine. *BIOCHEMICAL AND*
1007 *BIOPHYSICAL RESEARCH COMMUNICATIONS*, *8*(5), 377–382.
1008 https://doi.org/https://doi.org/10.1016/0006-291X(62)90011-6
1009 Nørholm, M. H. H. (2010). A mutant Pfu DNA polymerase designed for advanced
1010 uracil-excision DNA engineering. *BMC Biotechnology*, *10*(1), 21.
1011 https://doi.org/10.1186/1472-6750-10-21
1012 Ortiz, C., Natale, P., Cueto, L., & Vicente, M. (2015). The keepers of the ring:
1013 Regulators of FtsZ assembly. *FEMS Microbiology Reviews*, *40*(1), 57–67.
1014 https://doi.org/10.1093/femsre/fuv040
1015 Oswald, F., Varadarajan, A., Lill, H., Peterman, E. J. G., & Bollen, Y. J. M. (2016).
1016 MreB-Dependent Organization of the E. coli Cytoplasmic Membrane Controls
1017 Membrane Protein Diffusion. *Biophysical Journal*, *110*(5), 1139–1149.
1018 https://doi.org/10.1016/j.bpj.2016.01.010
1019 Pastoret, S., Fraipont, C., Blaauwen, T. Den, Aarsman, M. E. G., Thomas, A.,
1020 Brasseur, R., & Nguyen-diste, M. (2004). Functional Analysis of the Cell

Division Protein FtsW of *Escherichia coli*. *Journal of Bacteriology*, *186*(24), 8370–8379. https://doi.org/10.1128/JB.186.24.8370

Pedro, M. A. De, Quintela, J. C., Höltje, J. V, & Schwarz, H. (1997). Murein segregation in *Escherichia coli*. *Microbiology*, *179*(9), 2823–2834. https://doi.org/doi: 10.1128/jb.179.9.2823-2834.1997

Pichoff, S., & Lutkenhaus, J. (2002). Unique and overlapping roles for ZipA and FtsA in septal ring assembly in *Escherichia coli*. *EMBO Journal*, *21*(4), 685–693. https://doi.org/10.1093/emboj/21.4.685

Pichoff, S., & Lutkenhaus, J. (2005). Tethering the Z ring to the membrane through a conserved membrane targeting sequence in FtsA. *Molecular Microbiology*, *55*(6), 1722–1734. https://doi.org/10.1111/j.1365-2958.2005.04522.x

Pomorski, T., & Menon, A. K. (2006). Lipid flippases and their biological functions. *Cellular and Molecular Life Sciences*, *63*(24), 2908–2921. https://doi.org/10.1007/s00018-006-6167-7

Priyadarshini, R., De Pedro, M. A., & Young, K. D. (2007). Role of peptidoglycan amidases in the development and morphology of the division septum in *Escherichia coli*. *Journal of Bacteriology*, *189*(14), 5334–5347. https://doi.org/10.1128/JB.00415-07

Prosser, G. a, & de Carvalho, L. P. S. (2013). Kinetic mechanism and inhibition of *Mycobacterium tuberculosis* D-alanine:D-alanine ligase by the antibiotic D-cycloserine. *The FEBS Journal*, *280*(4), 1150–66. https://doi.org/10.1111/febs.12108

Qiao, Y., Srisuknimit, V., Rubino, F., Schaefer, K., Ruiz, N., Walker, S., & Kahne, D. (2017). Lipid II overproduction allows direct assay of transpeptidase inhibition by [beta]-lactams. *Nature Chemical Biology*, *13*(7), 793–798. https://doi.org/10.1038/nchembio.2388

Rico, A. I., García-Ovalle, M., Mingorance, J., & Vicente, M. (2004). Role of two essential domains of *Escherichia coli* FtsA in localization and progression of the division ring. *Molecular Microbiology*, *53*(5), 1359–1371. https://doi.org/10.1111/j.1365-2958.2004.04245.x

Rowlett, V. W., & Margolin, W. (2015). The Min system and other nucleoid-independent regulators of Z ring positioning. *Frontiers in Microbiology*, *6*(MAY), 1–10. https://doi.org/10.3389/fmicb.2015.00478

Ruiz, N. (2008). Bioinformatics identification of MurJ (MviN) as the peptidoglycan lipid II flippase in *Escherichia coli*. *Proceedings of the National Academy of Sciences of the United States of America*, *105*(40), 15553–7. https://doi.org/10.1073/pnas.0808352105

Ruiz, N. (2009). *Streptococcus pyogenes* YtgP (Spy-0390) complements *Escherichia coli* strains depleted of the putative peptidoglycan flippase MurJ. *Antimicrobial Agents and Chemotherapy*, *53*(8), 3604–3605. https://doi.org/10.1128/AAC.00578-09

Ruiz, N. (2015). Lipid Flippases for Bacterial Peptidoglycan Biosynthesis. *Lipid Insights*, *8*(Suppl 1), 21–31. https://doi.org/10.4137/LPI.S31783

Ruiz, N. (2016). Filling holes in peptidoglycan biogenesis of *Escherichia coli*. *Current Opinion in Microbiology*, *34*, 1–6. https://doi.org/10.1016/j.mib.2016.07.010

Sauvage, E., Kerff, F., Terrak, M., Ayala, J. A., & Charlier, P. (2008). The penicillin-binding proteins: Structure and role in peptidoglycan biosynthesis. *FEMS Microbiology Reviews*, *32*(2), 234–258. https://doi.org/10.1111/j.1574-6976.2008.00105.x

Scheffers, D. J., & Tol, M. B. (2015). LipidII: Just Another Brick in the Wall? *PLoS Pathogens*, *11*(12), 1–12. https://doi.org/10.1371/journal.ppat.1005213

Sham, L.-T., Butler, E. K., Lebar, M. D., Kahne, D., Bernhardt, T. G., & Ruiz, N. (2014). MurJ is the flippase of lipid-linked precursors for peptidoglycan biogenesis. *Science*, *345*(6193), 220–222. https://doi.org/10.1126/science.1254522

Shih, Y. L., Kawagishi, I., & Rothfield, L. (2005). The MreB and Min cytoskeletal-like systems play independent roles in prokaryotic polar differentiation. *Molecular Microbiology*, *58*(4), 917–928. https://doi.org/10.1111/j.1365-2958.2005.04841.x

Sieger, B., Schubert, K., Donovan, C., & Bramkamp, M. (2013). The lipid II flippase RodA determines morphology and growth in *Corynebacterium glutamicum*. *Molecular Microbiology*, *90*(5), 966–982. https://doi.org/10.1111/mmi.12411

Sun, Q., & Margolin, W. (1998). FtsZ Dynamics during the Division Cycle of Live *Escherichia coli* Cells, *180*(8), 2050–2056.

Suzuki, H., Nishimura, Y., & Hirota, Y. (1978). On the process of cellular division in *Escherichia coli*: a series of mutants of *E. coli* altered in the penicillin-binding proteins. *Proceedings of the National Academy of Sciences of the United States of America*, *75*(2), 664–668. https://doi.org/10.1073/pnas.75.2.664

Taschner, P. E., Huls, P. G., Pas, E., & Woldringh, C. L. (1988). Division behavior and shape changes in isogenic *ftsZ*, *ftsQ*, *ftsA*, *pbpB*, and *ftsE* cell division mutants of *Escherichia coli* during temperature shift experiments. *Journal of Bacteriology*, *170*(4), 1533–1540. https://doi.org/doi: 10.1128/jb.170.4.1533-1540.1988

Tsang, M. J., & Bernhardt, T. G. (2015). Guiding divisome assembly and controlling its activity. *Current Opinion in Microbiology*, *24*, 60–65. https://doi.org/10.1016/j.mib.2015.01.002

van der Ploeg, R., Goudelis, S. T., & den Blaauwen, T. (2015). Validation of FRET Assay for the Screening of Growth Inhibitors of *Escherichia coli* Reveals Elongasome Assembly Dynamics. *International Journal of Molecular Sciences*, *16*(8), 17637–54. https://doi.org/10.3390/ijms160817637

Van der Ploeg, R., Verheul, J., Vischer, N. O. E., Alexeeva, S., Hoogendoorn, E., Postma, M., … Den Blaauwen, T. (2013). Colocalization and interaction between elongasome and divisome during a preparative cell division phase in *Escherichia coli*. *Molecular Microbiology*, *87*(5), 1074–1087. https://doi.org/10.1111/mmi.12150

van Teeffelen, S., Wang, S., Furchtgott, L., Huang, K. C., Wingreen, N. S., Shaevitz, J. W., & Gitai, Z. (2011). The bacterial actin MreB rotates, and rotation depends on cell-wall assembly. *Proceedings of the National Academy of Sciences*, *108*(38), 15822–15827. https://doi.org/10.1073/pnas.1108999108

Vischer, N. O. E., Verheul, J., Postma, M., van den Berg van Saparoea, B., Galli, E., Natale, P., … den Blaauwen, T. (2015). Cell age dependent concentration of *Escherichia coli* divisome proteins analyzed with ImageJ and ObjectJ. *Frontiers in Microbiology*, *6*(JUN), 1–18. https://doi.org/10.3389/fmicb.2015.00586

Vollmer, W., Blanot, D., & De Pedro, M. A. (2008). Peptidoglycan structure and architecture. *FEMS Microbiology Reviews*, *32*(2), 149–167. https://doi.org/10.1111/j.1574-6976.2007.00094.x

Vollmer, W., Blanot, D., De Pedro, M. A., Scheffers, D., Pinho, M., Nikolaidis, I., … Dessen, A. (2005). Structural and mechanistic basis of penicillin-binding protein inhibition by lactivicins. *FEMS Microbiology Reviews*, *30*(2), 565–569.

https://doi.org/10.1128/MMBR.69.4.585
Wang, E., Walsh, C., & Walsh, C. (1978). Suicide substrates for the alanine racemase of *Escherichia coli*. *Biochemistry*, *17*(7), 1313–1321. https://doi.org/10.1021/bi00600a028
Weiss, D. S. (2015). Last but not least: New insights into how FtsN triggers constriction during *Escherichia coli* cell division. *Molecular Microbiology*, *95*(6), 903–909. https://doi.org/10.1111/mmi.12925
White, C. L., & Gober, J. W. (2012). MreB: Pilot or passenger of cell wall synthesis? *Trends in Microbiology*, *20*(2), 74–79. https://doi.org/10.1016/j.tim.2011.11.004
Wood, B. W. A., & Gunsalusa, I. C. (1959). D-Alanine formation; a racemase in *Streptococcus faecalis*. *Journal of Biological Chemistry*, *190*, 403–416.
Young, K. D. (2014). A flipping cell wall ferry. *Microbiology*, *345*(6193), 139–140. https://doi.org/10.1126/science.1256585
Yousif SY, Broome-Smith JK, S. B. (1985). Lysis of *Escherichia coli* by beta-lactam antibiotics: deletion analysis of the role of penicillin-binding proteins 1A and 1B. *J Gen Microbiol.*, *131*(10), 2839–45.

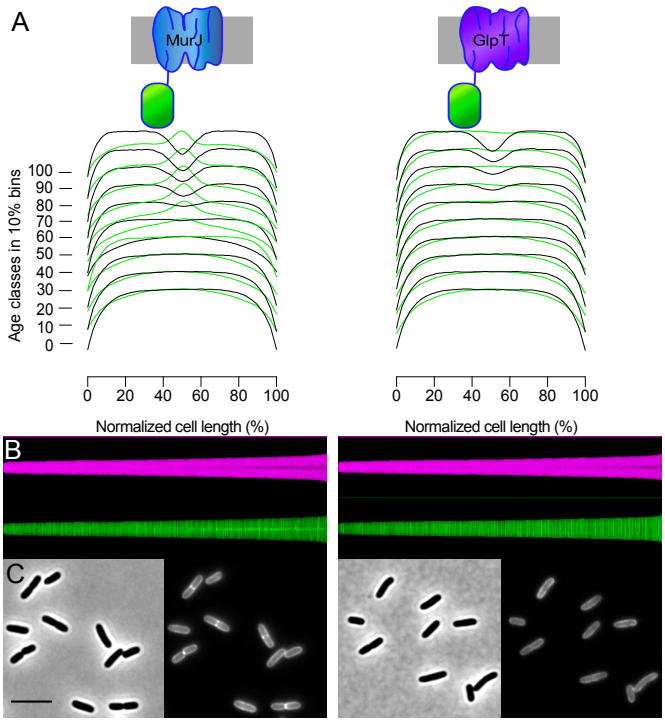

Figure legends

Fig. 1. MurJ localizes both in the lateral wall and at midcell. Strain XL08 containing the chromosomal mNG-MurJ fusion shows a cell-cycle-dependent localization in contrast to the homogenously localizing integral membrane protein mNG-GlpT. Cells were grown in Gb1 minimal medium to steady state at 28°C. Left: MurJ profiles; Right: membrane control protein GlpT profiles. (A) Collective profiles of localization of MurJ and GlpT. For each protein, the diameter (black lines) and fluorescence (green lines) profiles along normalized cell length are shown in 10 % age class bins. (B) Maps of diameter profiles (magenta) and fluorescence profiles (green). Cells are plotted by length, ascending from left to right. (C) Phase contrast image (left) and the corresponding fluorescence image (right) for each protein. Scale bar equals 5 μm. More than 1200 cells were included for both analyses.

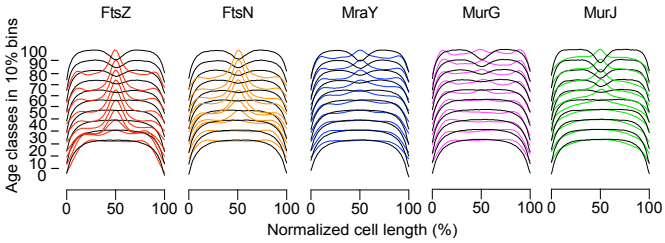

Fig. 2. Timing of MurJ midcell localization. mNG-$(GGS)_2$-MurJ cellular localization was compared with the localization of divisomal and PG precursor synthesizing proteins. XL08 strain was grown to steady state in Gb1 medium. MurJ localization was determined in living cells. After fixation with FAGA, the rest of cells were immunolabeled with antibodies against FtsZ, FtsN, MraY and MurG. Diameter (black lines) and Fluorescence (colored lines) profiles were plotted into 10 % age class bins along the normalized cell length in %. More than 1200 cells were included.

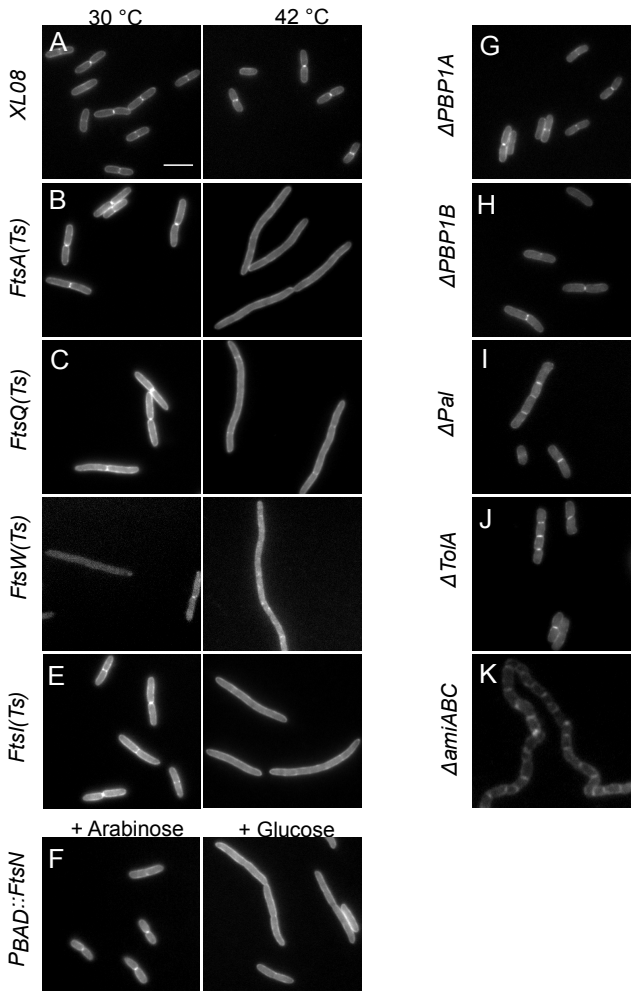

Fig. 3. MurJ requires the core divisome for its midcell localization. Chromosomal mNG-$(GGS)_2$-MurJ fusion was introduced into strains that harbor temperature sensitive, depletable, or deleted division proteins (except that the mNG-$(GGS)_2$-MurJ plasmid was expressed in *ΔtolA and Δpal strains, and the* mCherry-MurJ plasmid was expressed in *ΔamiABC* strain). (A-E) MurJ localization in XL08 (WT), *ftsA 1882* (Ts), *ftsQ1* (Ts), *ftsW* (Ts) and *ftsI2185* (Ts) backgrounds. Left: Localization at permissive temperature of 28 °C. Right: Localization after growth at the non-permissive temperature of 42 °C for 2 mass doublings (MD)s. (F) MurJ localization in FtsN depletion background at 30 °C. Left: localization in the presence of 0.2% w/v arabinose. Right: Localization of MurJ in the absence of arabinose for 2 MDs. (G-H) mCh-MurJ localization in *ΔmrcA* (PBP1A), *ΔmrcB* (PBP1B), *Δpal, ΔtolA* and *ΔamiABC* background at 30 °C, respectively. Scale bar equals 5 μm.

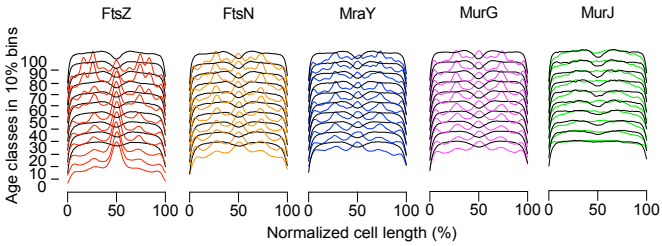

Fig. 4. Localization of cell division proteins in the presence of the PBP3 inhibitor aztreonam for 2 MDs. Cell division is inhibited but the localization and assemblage of the divisome continues, whereas the localization of MurJ is lost. In Gb1 at 28 °C, steady state growing XL08 was treated with 1 $mg.L^{-1}$ aztreonam, MurJ localization was determined in living cells, and FtsZ, FtsN, MraY and MurG were immunolabeled with antibodies after fixation. Diameter (black lines) and fluorescence (colored lines) profiles were plotted into 10 % age class bins along the normalized cell length. More than 1200 cells were included.

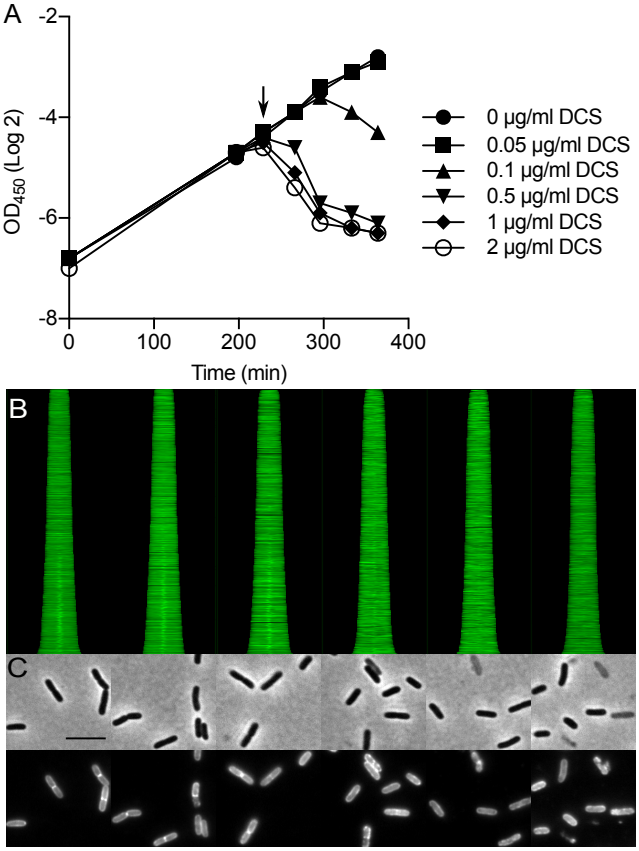

Fig. 5 Inhibition of lipid II biogenesis blocks MurJ midcell localization. In Gb1 at 28 °C, steady state growing XL08 was treated with increasing concentrations of D-cycloserine (DCS), and mNG-MurJ localization was determined at 30 minutes after addition of DCS. (A) Growth curves were plotted as time against the natural logarithm of the optical density of the cells. The black arrow indicates the addition of DCS. (B) Fluorescence maps profiles of MurJ localization. Cells are plotted according to increasing cell length from top to bottom. From left to right, the maps correspond to 0, 0.05, 0.1, 0.5, 1 and 2 µg.L^{-1} of DCS concentrations. More than 1200 cells were included. (C) Phase contrast images (upper) and correspond fluorescence images (down) of cells treated with DCS. Scale bar equals 5 µm.

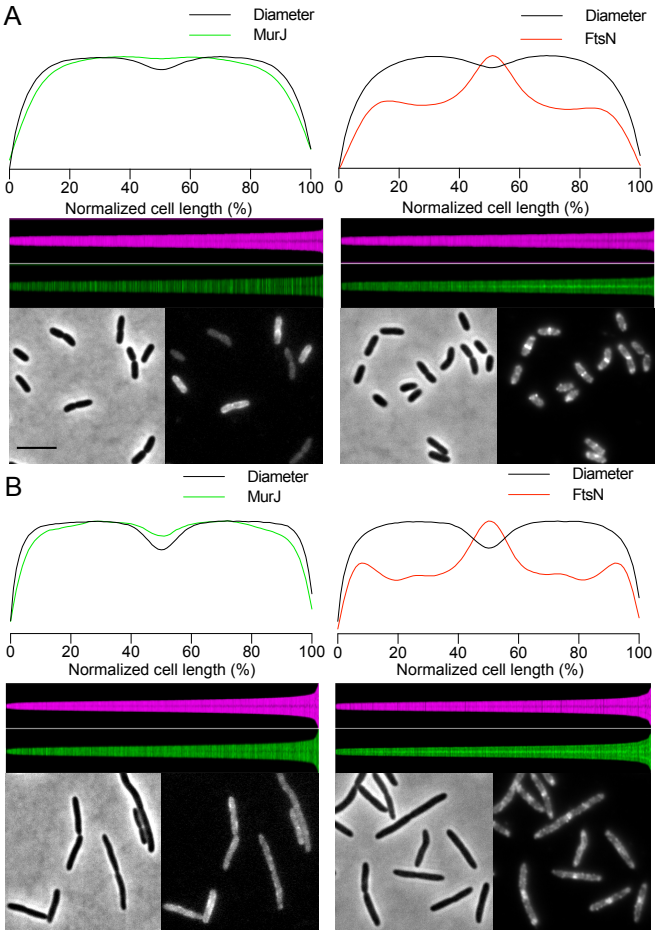

Fig. 6. Expression of non-functional FtsW mutants abolishes MurJ midcell localization. XL08 expressing mutant FtsW R145A or FtsW K153N was grown in Gb1 minimal medium to steady state at 28 °C. IPTG (20 μM) was used to induce expression of the FtsW mutants from plasmid. MurJ localization was determined in living cells and the presence of the divisome was confirmed by immunolabeling of FtsN, after fixation. (A) Localization of MurJ and FtsN after expression of FtsW R145A. (B) Localization of MurJ and FtsN after expression of FtsW K153N. For each part: top, average localization profiles plotted along normalized cell length (n ≥1200 cells). Black lines indicate cell diameter. Green lines and red lines indicate MurJ and FtsN localization, respectively. Middle, map profiles of cell diameter and MurJ or FtsN localization sorted by ascending cell length. Bottom, phase contrast and fluorescence microscopy images. Scale bar equals 5 μm.

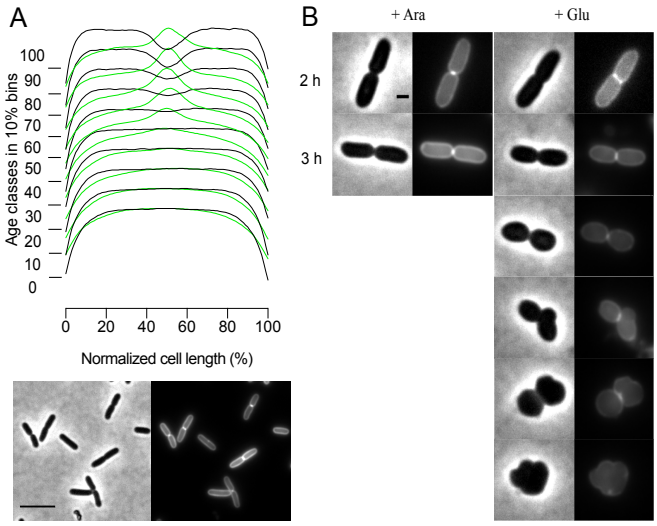

Fig. 7. MurJ non-functional mutant R18A does not influence its localization. (A) The plasmid expressing the mNG-MurJ R18A fusion was introduced into LMC500. This strain was grown in Gb1 minimal medium to steady state at 28 °C, and expression was induced with 20 μM IPTG for 2 MDs. The diameter (black lines) and fluorescence (green lines) profiles along normalized cell length are shown in 10 % age class bins. More than 1200 cells were included. Scale bar equals 5 μm. (B) The plasmid expressing the mNG-MurJ R18A fusion was introduced into the MurJ depletion strain XL20. Mutant localization was determined in the presence of arabinose (wild type MurJ expression) or glucose (wild type MurJ depletion). Scale bar equals 1 μm.

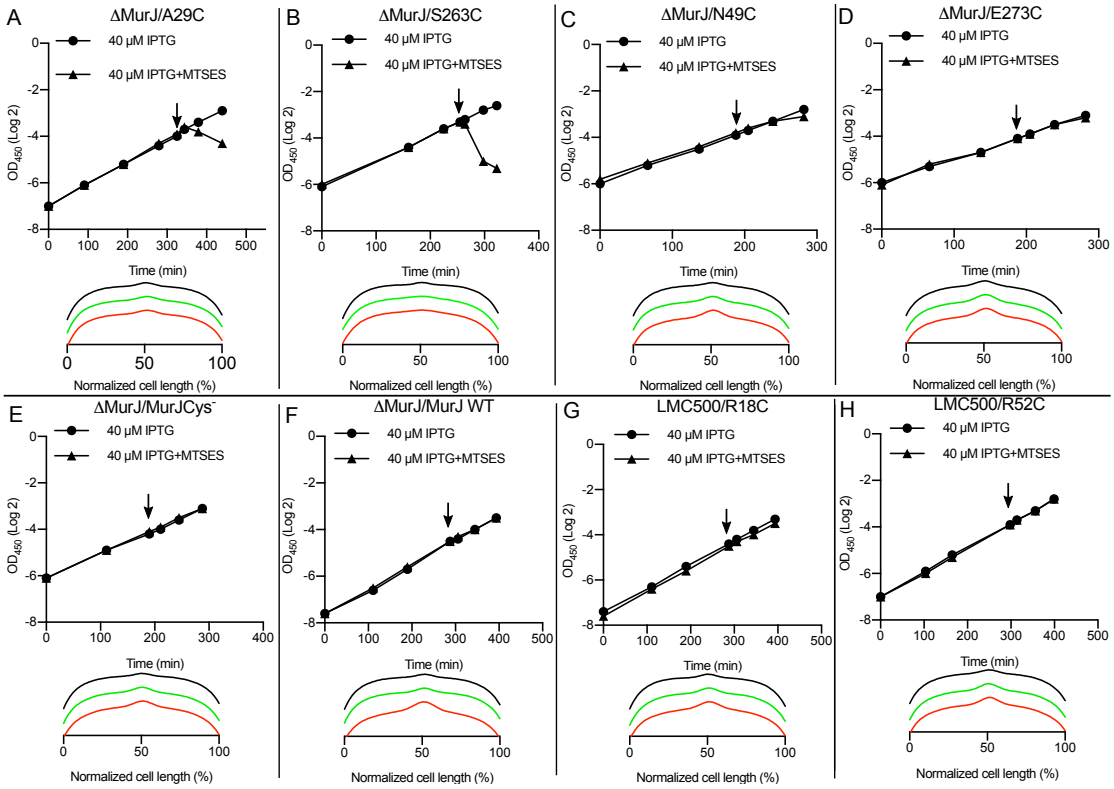

Fig. 8. Localization of MurJ cysteine mutants in the presence of MTSES. Strains expressing MurJ single-cysteine-mutants from plasmid were grown to steady state in Gb1 medium at 28 °C, and expression was induced with IPTG for 2 MDs. MurJ localization was determined at 10 min and 40 min after the addition of MTSES (for mutant S263C, localization was determined at 10 min and 20 min because of its higher sensitivity to MTSES), Average of MurJ localization profiles were plotted along normalized cell axis. Black lines indicate the MurJ localization in the absence of MTSES, green and red lines indicate the MurJ localization at 10 and 40 min in the presence of MTSES, respectively. More than 1200 cells were included for each experiment. (A-D) Only growth but not localization of functional mutants A29C, S263C, N49C and E273C is affected by MTSES. (E) Neither growth nor localization of cysteine free mutants is influenced by MTSES. (F) Neither growth nor localization of wild type MurJ is influenced by MTSES. (G and H) Localization of non-functional MurJ mutants R18C and R52C is not affected by MTSES.

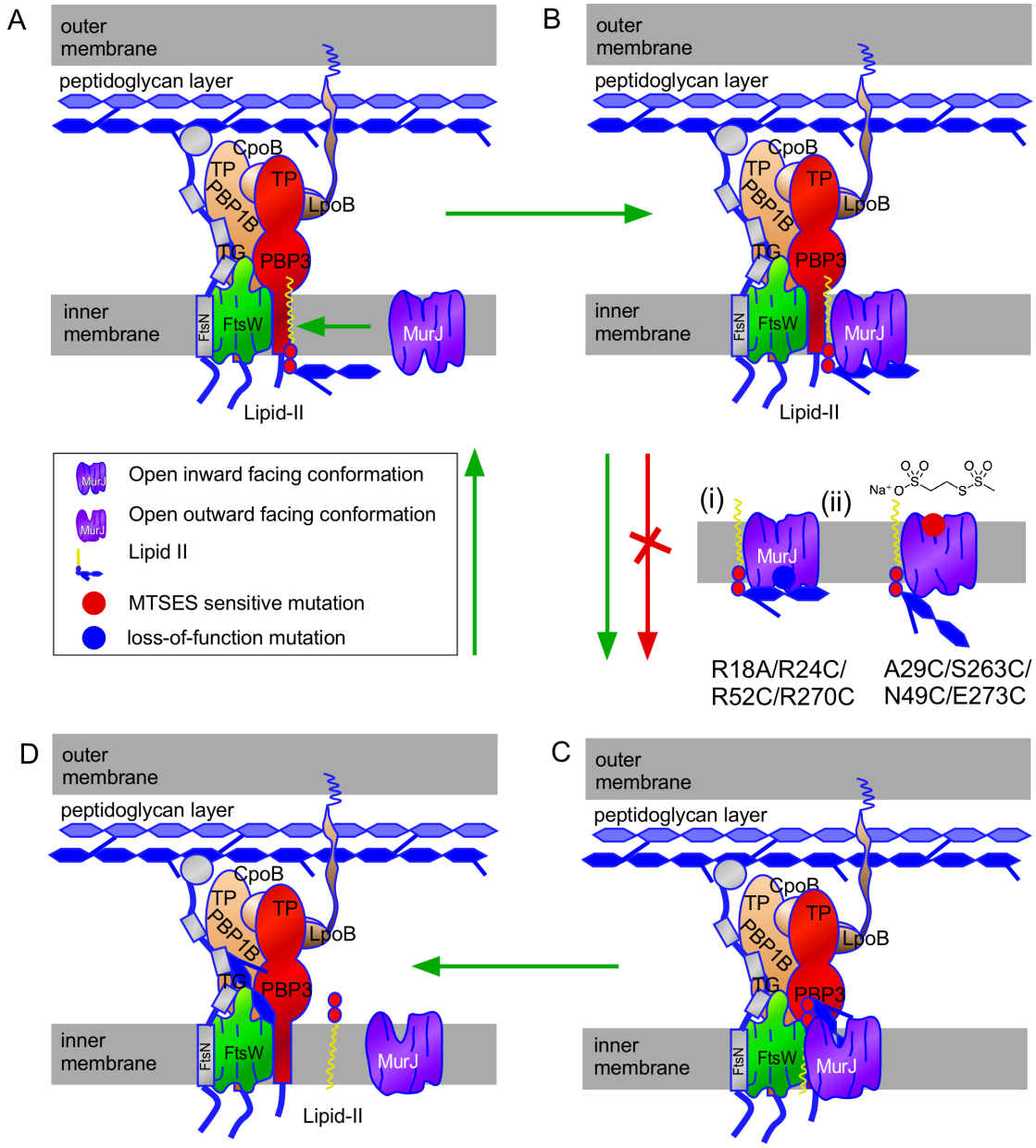

Fig. 9. Model of MurJ recruitment and function in septal peptidoglycan synthesis. (A) Recruitment of MurJ to midcell when FtsW is activated. (B) MurJ binds substrate. (C) MurJ flips lipid II across the IM by changing its structure from the inward-facing conformation into the outward-facing state. (D) Unloaded MurJ changes back into the default inward-facing state to participate in a new cycle. (i) Loss-of-function MurJ mutants that localize but are not able to flip lipid II. (ii) Functional MurJ mutants that are inactivated by MTSES still localize but are not able to flip lipid II.

1304 Table 1. Functionality and localization of MurJ fluorescence proteins fusions with different
1305 linkers at N- or C- terminus

Fusions	Plasmids	Complementation[a]	Localization[b]	Function[c]
No fusion	pTHV037-MurJ	≈16h	ND	+
	pSAV057-MurJ	≈16h	ND	+
N-terminus	pTHV037-mCh-$(GGS)_n$-MurJ	≈16h	+	+
	pSAV057-mNG-$(GGS)_n$-MurJ	≈16h	+	+
	pSAV057-mKO-MurJ	≈16h	+	+
C-terminus	pTHV037-MurJ-$(GGS)_n$-mCh	≥3 days	−	−
	pSAV057-MurJ-$(GGS)_n$-mNG	≥3 days	−	−

1306 n: Number of GGS repeats (n = 0, 1, 2, 3)
1307 [a] after transformation, the time period needed for visible white colony appearance.
1308 [b] +, FP fused MurJ is fluorescent and localizes in the membrane; −, FP fused MurJ is
1309 fluorescent and localizes in the cytosol.
1310 [c] +, functional fusion; −, loss-of-function fusion.